

Monitoring of DDO68 ‘Northern Ring’ SF regions during years 2016–2023

S.A. Pustilnik,^{1*} Y.A. Perepelitsyna,¹ A.S. Vinokurov,¹ E.S. Egorova,^{2,3} A.S. Moskvitin,¹
V.P. Goranskij,² A.N. Burenkov,¹ O.A. Maslennikova,¹ O.I. Spiridonova¹

¹ *Special Astrophysical Observatory of RAS, Nizhnij Arkhyz, Karachai-Circassia 369167, Russia*

² *Sternberg Astronomical Institute, Lomonosov Moscow State University, Universitetskij Pr. 13, Moscow 119992, Russia*

³ *Astronomisches Rechen-Institut, Zentrum für Astronomie der Universität Heidelberg, Mönchhofstraße 12-14, 69120 Heidelberg, Germany*

Accepted 2024 October 4, Received 2024 April 20

ABSTRACT

DDO68 is a star-forming (SF) dwarf galaxy residing in a nearby void. Its gas metallicity is among the lowest known in the local Universe, with parameter $12+\log(\text{O}/\text{H})$ in the range of 6.96–7.3 dex. Six of its SF regions are located in or near the so-called ‘Northern Ring’, in which the Hubble Space Telescope (HST) images reveal many luminous young stars. We present for these SF regions (Knots) the results of optical monitoring in 35 epochs during the years 2016–2023. The data was acquired with the 6m (BTA) and the 1m telescopes of the Special Astrophysical Observatory and the 2.5m telescope of the MSU Caucasian Mountain Observatory. We complement the above results with the archive data from 10 other telescopes for 11 epochs during the years 1988–2013 and with 3 our BTA observations between 2005 and 2015. Our goal is to search for variability of these Knots and to relate it to the probable light variations of their brightest stars. One of them, DDO68-V1 (in Knot 3), was identified in 2008 with a luminous blue variable (LBV) star, born in the lowest metallicity environments. For Knot 3, variations of its integrated light in the previous epochs reached ~ 0.8 mag. In the period since 2016, the amplitude of variations of Knot 3 reached ~ 0.3 mag. For the rest Knots, due to the lower amplitudes, the manifestation of variability is less pronounced. We examine the presence of variability via the criterion χ^2 and the Robust Median Statistics and discuss the robustness of the detected variations. The variability is detected according to the both criteria in the lightcurves of all Knots with the χ^2 confidence level of $\alpha = 0.0005$. The peak-to-peak amplitudes of variations are ~ 0.09 , ~ 0.13 , ~ 0.11 , ~ 0.08 and ~ 0.16 mag for Knots 1, 2, 4, 5 and 6, respectively. The amplitudes of the related variations of the brightest supergiants in these regions can reach of ~ 3.0 mag.

Key words: stars: massive – stars: variables: general – stars: individual (DDO68-V1) – stars: metallicity – galaxies: individual: DDO68 (UGC5340, VV542)

1 INTRODUCTION

Massive stars (conditionally, of 8 to 100 and more M_{\odot}) are very important element of several interrelated directions in astrophysics, from star formation and its feedback, galaxy formation and evolution to cosmological issues related to reionisation of the intergalactic medium. Due to their short life timescale, the massive stars in the Galaxy have metallicities close to the current gas metallicity, that is close to $Z \sim Z_{\odot}$.

There are several tasks related to the study of massive stars in the context of the diverse metallicity. In particular, the understanding of properties of massive stars with very low Z of $\lesssim Z_{\odot}/30$ is crucial for studying and modelling of galaxy formation and evolution at the epoch of dawn of the Universe. The need to check the modern models of massive very low- Z stars on the real objects assumes the search for and study such objects in the outer galaxies.

The gas metallicity in the nearby Universe was found to vary in the range of (~ 0.02 – 3) Z_{\odot} . Due to the well-known relation between mass (or luminosity) and gas metallicity in late-type galaxies, the lowest metallicity massive stars

* sap@sao.ru (SAP)

are expected to form currently in dwarf galaxies. According to the statistical relation between the gas metallicity and galaxy luminosity for late-type galaxies within the Local Volume (LV) (Berg et al. 2012), dwarf galaxies with the gas metallicity (and hence, that of young massive stars) of $Z \lesssim Z_{\odot}/30$ (eXtremely Metal-Poor, hereafter, XMP) should be rather faint, with $M_B \gtrsim -9$ mag. Such faint dwarfs and their massive stars are accessible only at the distances of the LV and its environs. The nearest dwarf with that low metallicity, Leo P (Skillman et al. 2013), possesses the only HII region, excited by one O7-8 V star. It was recently studied by Telford et al. (2023). To substantially advance in the studying of massive stars at such extremely low Z (including the massive stars in the evolved stages), one needs XMP galaxies with many massive stars within the LV (Garcia et al. 2021).

According to our spectral study of void galaxies (Pustilnik et al. 2016, 2020, 2021, 2024), the XMP dwarfs favour the void environment. Moreover, for a given luminosity, they show substantially reduced gas metallicities. And visa versa, for their extremely low metallicities, they appear substantially more luminous than one would expect from the reference relation of Berg et al. (2012), derived for galaxies in the denser environment. Therefore, statistically, the probability to find multiple massive stars in void XMP dwarfs is higher than for the similar dwarfs outside voids.

Luminous blue variable (LBV) stars are thought to represent a relatively short transient and rather unstable stage of massive star evolution from the main sequence hydrogen burning O-stars to the core-helium burning Wolf-Raye (WR) stars (Humphreys & Davidson 1994). During this stage, massive stars lose the substantial mass via the powerful wind and in a series of 'normal' eruptions with the typical timescales of a few years per event. Besides, some evidence appeared that LBVs can also be the direct precursors of supernova Type II explosions (e.g., Petrov, Vink, Gräfener 2006, and references therein).

The nature of variable massive star winds is better understood for the solar and subsolar metallicities, for which the wind power scales with metallicity Z, indicating the dominant role of radiation pressure to ions of metals (e.g. Vink 2022). Extrapolation of such wind mechanism to very low metallicities assumes no WR stars in the most metal poor starburst. However, the detection of WR population in the most metal-poor BCGs (e.g. Guseva et al. 2000)) evidence that other mechanisms may operate for massive star winds at the very low metallicities. Moreover, for the most dramatic events known as LBV 'giant eruptions', the radiation pressure mechanism may be not suitable (e.g. Smith & Owocki 2006).

Hence, the study of individual very low-Z massive stars can be crucial for the choice of their most reliable models. The understanding of processes in very metal-poor LBVs is especially suitable since due to their highly non-stationary mass loss, their properties should be more sensitive to the model assumptions.

The recent studies of massive stars with metallicities as low as $Z = Z_{\odot}/10$ in Sextans A (Lorenzo et al. 2022; Schootemeijer et al. 2022), and $Z = Z_{\odot}/20$ in Leo A (Gull et al. 2022), represent the important steps in understanding the properties of the low-metallicity massive stars. However, the search for opportunities to study massive stars

at even lower Z, say at $Z_{\odot}/50 - Z_{\odot}/40$, still remains highly challenging.

The number of individual very massive stars in galaxies with the extremely low metallicity ($Z \lesssim Z_{\odot}/30$, corresponding to the host SF regions with the gas oxygen abundance of $12+\log(\text{O}/\text{H}) \lesssim 7.2$ dex) is very limited in the local Universe. Even more so it relates to such low-Z massive stars at the *advanced* evolutionary stages. They, first of all, include a number of WR stars and red supergiants (RSGs) in the prototype XMP dwarf IZw18 (e.g. Izotov et al. 1997; Legrand et al. 1997; Hirschauser et al. 2024) at $D \sim 16$ Mpc.

Another important object is the dwarf XMP galaxy DDO68 at $D = 12.75$ Mpc ($\mu = 30.53$ mag) (Makarov et al. 2017; Cannon et al. 2014), as derived via the TRGB method. In this galaxy, the lowest metallicity LBV star was discovered (also known as DDO68-V1) (Pustilnik et al. 2008; Izotov & Thuan 2009) along with many identified individual supergiants (Pustilnik et al. 2017).

The Lynx-Cancer void galaxy DDO68 (UGC5340, VV542) is known as a peculiar morphology, the almost record-low metallicity (average $12+\log(\text{O}/\text{H})=7.14$) dIrr with several prominent young star-forming (SF) regions. Most of these SF regions are found at the periphery, mainly in the 'Northern ring' and the 'Southern tail' (Pustilnik et al. 2005; Izotov & Thuan 2007). These SF regions, named Knots in Pustilnik et al. (2005), look in fact as young OB associations hosting tens massive stars, with the typical linear sizes of several tens pc. The only exception is the compact Knot 5, which shows properties of a young globular cluster with the age of about 20 Myr. See the HST image of Knots 1–6 in Fig. 1.

Annibali et al. (2019) found the range of metallicities in DDO68, from $12+\log(\text{O}/\text{H}) \sim 7.3$ dex near the center of the main body, down to ~ 7.0 dex in the southernmost SF region. The importance of this XMP dwarf in the context of the future study of the lowest metallicity massive stars was first emphasised about 20 years ago by Kniazev, Pustilnik (2006). Thanks to good luck, the unique Luminous Blue Variable star (LBV) was discovered in the repeat observations of DDO68, in one of the most metal-poor SF regions in the local Universe (Pustilnik et al. 2008; Izotov & Thuan 2009).

The issue of the extremely metal-poor massive star evolution and death remains one of the clues for understanding of galaxy formation and evolution for the time of $\lesssim 1$ Gyr since the Big Bang (e.g., Barkana & Loeb 2001; Eldridge, Stanway 2022). This is especially actual in the epoch of active observational exploration of galaxies for the time of 0.5 – 1 Gyr since the Big Bang with the James Webb Space Telescope (JWST). The great majority of these remote objects are star-forming galaxies. They display a wide range of metallicities, including the lowest values, found in the local Universe (e.g. Maseda et al. 2023).

While the state-of-art stellar evolution models, including those with the fast rotation, have substantially advanced during the last decade (e.g. Szecsi et al 2015; Chen et al. 2015; Sanyal et al. 2017; Martins, Palacios 2021, and references therein) the direct comparison of the model predictions with properties of real extremely metal-poor massive stars is still absent. The main reason is the lack of such stars in the local Universe which would be accessible for sufficiently detailed studies. One needs to wait for the qual-

itative progress, expected for the upcoming extremely large next generation optical telescopes. As a preliminary step for these future studies, the search for such rare massive stars and examination of their available properties, such as variability, appears valuable and necessary.

As explained above, the main goal of the monitoring of the DDO68 'Northern Ring' region is an attempt to examine the possible peculiarities in the light curve of the extremely metal-poor LBV DDO68-V1. However, the images used for this task, cover the five other SF regions (Knots), in which the HST data allow us to separate many other massive stars. In particular, the list of the 50 brightest stars (super-giants with $M_V \leq -6.0$ mag) in these Knots was presented in Pustilnik et al. (2017). Their sufficiently large-amplitude variability can, in principle, be detected via variations of the integral light of their host SF regions.

The mentioned above SF regions, excluding Knot 5, are rather young, as follows from their large values of the equivalent widths of the emission $H\beta$ (Pustilnik et al. 2005). With the range of $EW(H\beta) = 47 - 250 \text{ \AA}$, the respective ages of the instantaneous star-bursts correspond to the range of 3–7 Myr (Leitherer et al. 1999). So that one can expect the population of massive OB stars at various evolutionary stages still alive. Their non-stationary stellar wind activity can manifest as a substantial light variability.

In this paper we present the most updated lightcurve for Knot 3, containing the most metal-poor LBV star DDO68-V1. The data will be used in the forthcoming paper, examining the LBV light variations after its so-called 'giant eruption' in 2010–2013 years. More emphasis in the paper is given to the 'by-product' – monitoring the light variations in the rest Knots. We present at the first time the magnitudes and lightcurves of Knots 1, 2, 4, 5 and 6 and examine them for the possible signs of variability using the well-known χ^2 criterion and the so-called RoMS (Robust Median Statistics, Rose, Hintz (2007); Burdanov et al. (2014)).

The lay-out of the paper is as follows. In Sect. 2 we present all the used observational data and briefly describe their reduction. In Sect. 3 the main results of data processing and analysis are presented. Sect. 4 describes arrays of photometric serieses for all Knots and their check for possible variability. Sect. 5 is devoted to discussion of new results, their comparison with the previous data and understanding them in a wider context. In Sect. 6 we summarise the new results and draw the main conclusions. The adopted linear scale is 62 pc in 1 arcsec.

2 OBSERVATIONAL DATA AND REDUCTION

2.1 BTA telescope data

The imaging of the mentioned above SF regions (Knots 1–6) was conducted with the multimode device SCORPIO-1 (Afanasiev, Moiseev 2005) at the prime focus of the SAO 6-m telescope (BTA). The parameters of observations are shown in the Journal (Tab. 1). The details of observations are given in our papers PKP05; Pustilnik et al. (2008) and Pustilnik et al. (2017). SCORPIO-1 with the CCD detector $2K \times 2K$ EEV 42-40 was used in the imaging mode. The images with the field of view with diameter of 6 arcmin, were obtained in the binning mode of 2×2 , with the scale of $0.356 \text{ arcsec pixel}^{-1}$.

2.2 SAO 1m telescope data

We performed observations (B , V and R passbands) during the years 2016 - 2023 with the 2048×2048 CCD photometer on the 1-m telescope of SAO RAS. The detector was CCD-EEV 42-40 with the full imaged field of ~ 7.3 arcmin and the scale (after binning of 2×2) of $0.432 \text{ arcsec/pixel}$.

The observations were conducted in the nights with multi-program schedules. Therefore, the images of DDO68 were obtained mainly in V -band. When there was an opportunity, the images in B and/or R -bands were also acquired. The log and parameters of observations are presented in the general journal of observation in Table 1 and indicated in the 4-th column as '1m'.

2.3 CMO 2.5m telescope data

We performed observations (in V and R passbands) at 2.5-m telescope of Caucasian Mountain Observatory (CMO) of Moscow State University in 2017–2019. We used 4296×4102 NBI camera (made in the Niels Bohr Institute, Copenhagen) (Shatsky et al. 2020) mounted in the Cassegrain focus of the telescope. The camera has a 10×10 arcmin field of view and scale of $0.16 \text{ arcsec/pixel}$.

Three observations of DDO68 were obtained during this period. Two images were acquired in V -band. The first - in April 2017, with the total exposure time of 25 minutes, and the second - in February 2018, with the total exposure time of 30 minutes. The third image was obtained in R band in January 2019 during the Moon time, with the total exposure time of 30 minutes. See details in Table 1.

2.4 Literature and archival data

In addition to our new photometry obtained with SAO 6m and 1m telescopes and 2.5m telescope of MSU, presented in Table 1, we use also the available archive CCD images, which we analysed in the similar way. In Table 2 we present the summary of imaging observations of DDO68 based on archives of nine ground-based telescopes world-wide and the HST data. Below we briefly comment on the origin of this data and refer to the papers, in which the respective programs and related issues are described in more detail.

2.4.1 Calar Alto 3.5-m telescope data

The observations of galaxy DDO68 were collected with the Prime focus CCD camera of the Calar Alto 3.5-m telescope in dark time on the night 1988.02.14 under photometric conditions by Hopp & Schulte-Ladbeck (1995). A RCS high resolution chip was used with the field of view of 256 by 160 arcsec and a resolution of 0.5 arcsec/pixel . For DDO68, the images were obtained in B -band and R -band, with the exposure times of 900 s and 600 s, respectively. Seeing was 1.1 arcsec . The program observations were accompanied by the appropriate CCD calibration observations (bias and dark frames and sky flats). After de-biasing, the dark current was subtracted, bad columns were removed, and the frames were flat-field corrected.

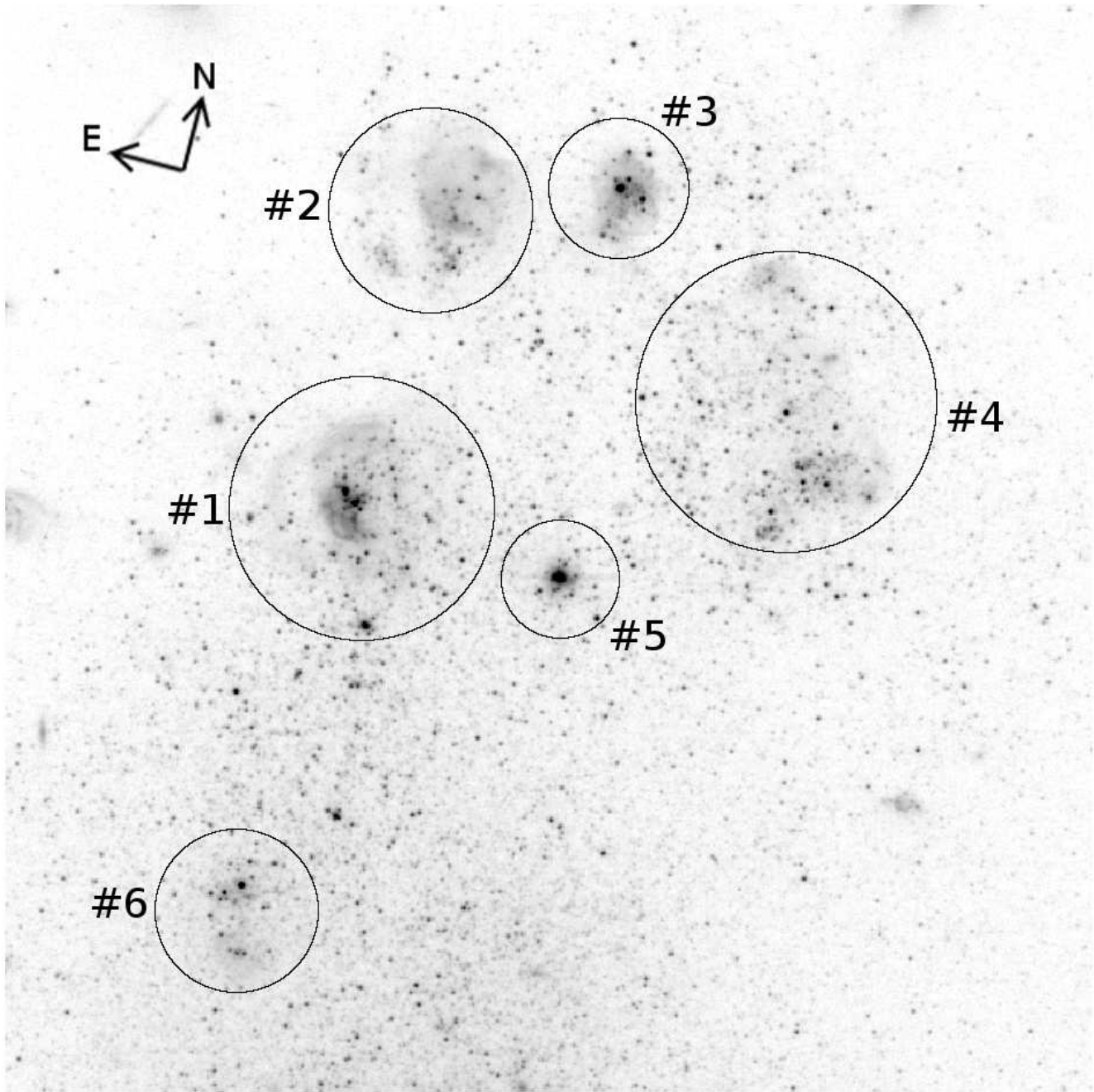


Figure 1. The part of the HST image of DDO68 in F606W filter centred on the 'Northern Ring' (Knots 1–5), including Knot 6 to the SW, with the used apertures superimposed. Image was acquired on 2010.05.01 for the HST program ID11578 (PI Aloisi). The diameters of the apertures (in arcsec) are as follows: Knot 1 (10.0), Knot 2 (8.0), Knot 3 with DDO68-V1 in the center (5.0), Knot 4 (11.0), Knot 5 (4.4), Knot 6 (6.0).

2.4.2 Isaac Newton 2.54-m telescope data

The image of DDO68 was obtained on 1994.02.05 by Swaters & Balcells (2002) with Johnson-Cousins R-band filter at seeing of 1.86 arcsec with the exposure time of 1200 s. The detector was CCD-EEV 4K×2K (EEV XHIP) with scale of 0.549 arcsec/pixel.

2.4.3 Nordic Optical (NOT) 2.56-m telescope data

Observations of DDO68 were carried out on 1995.02.07 on the program of Makarova & Karachentsev (1998) with the NOT 2.56-m telescope (La Palma). Images in B and V bands were obtained with the exposure times of 300 s and 300 s, and seeings of 0.9 and 0.7 arcsec, respectively. A CCD camera with a TEC 1k×1k chip provided a field of view of 3×3 arcmin, with the image scale of 0.176 arcsec/pixel.

Table 1. Journal of SAO and CMO observations of DDO68

Date	Band	Expos. time, s	Tel	β''
(1)	(2)	(3)	(4)	(5)
2005.01.12	V, R	1800,1800	BTA	1.7
2009.01.21	V	300	BTA	1.3
2015.01.14	B, V, R	300,360,360	BTA	2.1
2016.03.07	V	4200	1m	2.1
2016.03.08	B, V, R	1200,1200,1200	1m	2.1
2016.04.07	V	4200	1m	2.2
2016.05.17	V	4200	1m	2.2
2016.10.22	V	3600	1m	1.8
2016.11.24	B, V, R	3600,3600,3600	1m	1.9
2016.12.24	V	3600	1m	2.6
2016.12.31	V	5400	1m	1.6
2017.04.18	V	1500	CMO	1.7
2017.05.29	V	1200	1m	1.7
2017.11.16	B, V, R	600,600,600	BTA	1.9
2018.02.19	V	1800	CMO	1.8
2018.04.05	B, V, R	2100,2400,3900	1m	1.8
2018.04.30	V, R	2400,2400	1m	1.7
2018.10.11	V	3300	1m	1.6
2019.01.18	R	1800	CMO	1.0
2019.02.03	V	3600	1m	1.6
2019.10.26	B, V, R	600,600,600	BTA	1.2
2019.11.25	V	3600	1m	1.6
2020.01.19	R	1200	BTA	1.2
2020.01.20	B, V	600,600	BTA	1.5
2020.03.04	V, R	2400,1500	1m	1.7
2020.04.26	R	600	BTA	2.0
2020.11.11	V, R	600,900	BTA	1.5
2021.05.14	V	2400	1m	2.0
2021.05.16	R	1200	1m	2.0
2021.12.02	V, R	720,720	BTA	1.6
2022.04.26	V	3000	1m	1.7
2022.10.25	V, R	2700,1500	1m	2.5
2022.12.20	B, V, R	720,720,720	BTA	1.8
2022.12.25	B, V, R	1500,3600,2700	1m	2.2
2023.01.23	B, V, R	3600,3600,3600	1m	2.1
2023.03.18	V	2700	1m	1.9
2023.10.12	V	3600	1m	1.7
2023.10.22	V	900,900	BTA	1.9

2.4.4 Keck II 10-m telescope data

Observations of DDO68 were carried out on the night of 1997.12.23 with the Low Resolution Imaging Spectrometer (LRIS) at the f/15 Cassegrain focus of the Keck II telescope by Mendez et al. (2002). The used back-side-illuminated Tektronix 2048×2048 CCD detector had an image scale of 0.215 arcsec/pixel and a field of view of 6×8 arcmin. The images were obtained in V-band with the exposure time of 600 s, seeing of 1.0 arcsec and with the airmass of 1.02.

2.4.5 KPNO 4-m telescope data

The KPNO 4-m telescope images for DDO68 were obtained on the night 1998.02.17 in the frame of the program from the paper by Hunter & Elmegreen (2006). The 2K×2K Tektronix CCD images in B and V bands were acquired at see-

Table 2. Summary of archive data for DDO68

Date	Telescope	Band	Expos. time, s	β''
(1)	(2)	(3)	(4)	(5)
1988.02.14	3.5m CA	B, R	900,600	1.1
1994.05.02	2.54m INT	R	1200	1.9
1995.02.07	2.56m NOT	B, V	300,300	0.9
1997.12.23	10m KeckII	V	600	1.0
1998.02.17	4m KPNO	B, V	600,600	2.5
2000.04.07	1.8m VATT	B, V, R	600,480,360	1.7
2004.04.16	2.5m APO	g, r, i	57,57,57	1.4
2007.02.09	2.1m KPNO	g, i	1800,1800	0.9
2010.05.02	2.6m HST	V, I	7644,7644	0.1
2011.03.05	0.9m KPNO	B, V, R	900,600,420	1.4
2013.02.17	0.9m KPNO	B, V, R	1200,1200,1200	1.9

ing of 2.5 arcsec with the exposure time of 600 s. Scale at detector was 0.26 arcsec/pixel.

2.4.6 VATT 1.8-m telescope data

Images of DDO68 on 2000.04.07 were obtained with the Vatican 1.8 m telescope (VATT, see for more detail in Taylor et al. (2005)), located at Mt. Graham International Observatory (MGIO, Arizona, USA), with the 2K×2K Direct Imager. Exposure times in B, V, R filters were 600, 480, 360 s, respectively, at seeing of 1.5 – 1.8 arcsec. Scale on the detector was 0.374 arcsec/pixel.

2.4.7 KPNO 2.1-m telescope data

The images of DDO68 on 2007.02.09 were obtained with the KPNO 2.1-m telescope (Izotov & Thuan 2009) in the SDSS filters g and i, with the exposure time for both filters of 3×600 s. Airmass during observations was 1.05, with seeing of 0.9 arcsec. The used detector was Tektronix 2K×2K imager with the scale of 0.27 arcsec/pixel. The obtained magnitudes in g and i filters were transformed to that in V-band with the equations of Lupton et al. (2005).

2.4.8 The 2.6-m Hubble Telescope data

Imaging with the HST were obtained on 2010.04.30 (F814W) and 2010.05.02 (F606W) within the Program ID GO 11578 (PI A.Aloisi). The Advanced Camera for Surveys was used. The data processing and photometry for Knot 3 were already described in Pustilnik et al. (2017). For the other Knots, all aperture photometry was done similarly, with the same diameters of aperture as for the ground-based observations. The relatively large error of V-band magnitude of 0.08 mag is due to the related uncertainty of the transform from the HST filter magnitudes to Johnson - Cousins V-band magnitudes. For the concrete HST image, from which we derive V-band magnitudes of all our Knots, this rms transform 'error' will cause the same systematic shift for all Knots. If the value of such a shift is comparable to the

amplitude of the real variations of ~ 0.1 mag, this can manifest in the lightcurves of the Knots as a correlated uprise or decline.

2.4.9 KPNO 0.9-m telescope data

Observations of DDO68 with the Kitt Peak National Observatory's 0.9 meter telescope were carried out on the nights 2011.03.05 and 2013.02.17 in B, V, R bands (Cook et al. 2014). No publication was found in the literature related to the latter data. The S2KB detector was a 2048×2048 CCD mounted at the $f/7.5$ focus of the telescope. The field size was approximately of 20 arcmin on a side, with the scale of 0.6 arcsec/pixel.

2.5 Details of photometry

To derive the total magnitudes of the DDO68 Knots 1–6 in the 'Northern ring', we used MIDAS¹-based programs to perform the standard photometric pipeline with bias subtraction, flat-fielding and illumination correction. The background was approximated by the 2D polynomial of the 2nd degree. This was fitted on the data for ~ 80 small apertures around the Northern Ring, with the total area close to that of the Ring.

We neglect in the further estimates of the magnitude errors the component from the dark current and the read-out noise, since they are many times smaller than the contribution of Poisson noise from the sky background and an object. Adopting that the standard deviation of the Poisson process with N counts² is \sqrt{N} , the relative error of the object (Knot) flux is read as: $\sqrt{N_{\text{sky}+\text{obj}}} / N_{\text{obj}}$ where N_{sky} - number counts of sky within the used aperture, $N_{\text{sky}+\text{obj}}$ - number counts of sky together with the object. $N_{\text{obj}} = N_{\text{sky}+\text{obj}} - N_{\text{sky}}$, the difference number counts, the pure object counts. The subtraction of N_{sky} , fitted by the above polynomial, increases the Poisson standard deviation of the signal within the aperture on the object only by a few per cent.

For instrumental magnitudes, $m_{\text{inst}} = -2.5 \log(N_{\text{obj}})$, their respective errors σ_{inst} , assuming that they are small, are calculated as follows: $\sigma_{\text{inst}} = 2.5 \log(1 + \sqrt{N_{\text{sky}} + N_{\text{obj}}} / N_{\text{obj}})$ (1).

The photometry of DDO68 Knots 1–6 was based on the local standard stars. To transform the instrumental magnitudes to the apparent magnitudes in the respective bands, we used the zero-points determined for every image through the measurements of 5–6 or more local standard stars. These sufficiently bright stars ($g = 17.9 - 21.1$ mag) were selected in the Sloan Digital Sky Survey (SDSS DR7; Abazajian et al. 2009) images in the close vicinity of DDO68 so that they fall within the typical fields of view of our used images ($\gtrsim 6$ arcmin across). Their g, r, i magnitudes were measured independently with the aperture photometry and were transformed to the Johnson-Cousins B, V, R magnitudes according to the Lupton et al. (2005) relations.

These local standard stars are presented in Table 3, where we give their SDSS names, g, r, i magnitudes and the adopted Johnson-Cousins B, V, R magnitudes.

The apertures, used for the local standards, had radii from 2.1 to 3.1 arcsec and were adjusted in order to minimise the contribution of the local faint neighbours. The related small corrections to the asymptotic value of magnitude, depending on the seeing, were applied similar to those for the Knots. To find these corrections, we used the original HST images and smoothed them with the Gaussian filter corresponding to seeings between 1.0 to 2.5 arcsec. In each case, to obtain the total magnitude of the studied Knots, we used the round apertures with the fixed diameters, indicated in Table 4.

2.6 Errors budget

In Sect. 4 we perform the statistical checks of the Null hypothesis about the absence of variability in the photometric time serieses of the studied DDO68 Knots. These tests are based on the measurement errors, assuming that we have their correct estimates and all systematic and non-random factors are excluded. We briefly summarise the error estimate procedure and outline the issues which could potentially affect the errors of photometry.

The main advantage of our photometry was the use of the number of local standards what allowed us to define the zero-points (as the weighted mean on several standards) for every measurement. The errors of these weighted means in V-band fall between 0.002 and 0.016 mag, with the median of ~ 0.007 mag, and 3/4 of them of smaller than 0.012 mag. This estimate of the error of a zero-point was combined in quadrature with the relative error of the measured flux for the respective Knots. The errors for the zero-point in B-band fall between 0.002 and 0.023 mag, with the median error of ~ 0.008 mag. Similarly, for R-band, the errors of the zero-point fall between 0.002 and 0.018 mag, with the median of ~ 0.008 mag.

As mentioned in Sect. 2.5, the relative error of the measured flux is determined by the Poisson noise term shown under \sqrt{N} in formula (1) above. For all Knots, the term N_{sky} is larger than N_{obj} by a factor of $\sim 3-10$ in B-band, $\sim 5-10$ in V-band and ~ 15 in R-band. Therefore the contribution from an object to the Poisson noise is typically smaller than 10–20 per cent. Subtraction of the sky background, approximated by the 2D polynomial, as described above, increased the standard deviation in the resulting image only by a few per cent. So, we ignored this small addition of the noise.

For the typical time exposures per filter of 10 minutes at BTA, for case of Knot 3, the faintest of all six Knots (see Table 4), the respective numbers of N_{sky} are $\sim 3.6 \times 10^5$, $\sim 5.6 \times 10^5$ and $\sim 1.1 \times 10^7$ in B, V and R-bands, respectively. The respective counts of N_{obj} in B, V and R bands were $\sim 1.3 \times 10^5$, $\sim 1.0 \times 10^5$ and $\sim 6.6 \times 10^5$. The typical error of the instrumental magnitudes, of σ_{inst} are 0.006, 0.009 and 0.006 mag in the respective bands.

For observations at the SAO 1m telescope, with the typical exposure time of 60 minutes, the respective numbers of N_{sky} are $\sim 4.8 \times 10^5$, $\sim 7.5 \times 10^5$ and $\sim 1.8 \times 10^6$ in B, V and R-bands, respectively. The respective counts of N_{obj} in B, V and R band were $\sim 5.5 \times 10^4$, 7.0×10^4 and 6.5×10^4 . The

¹ MIDAS is an acronym for the European Southern Observatory package – Munich Image Data Analysis System

² Here N is the detector electron number counts, that is ADU counts multiplied by 'gain'.

related typical errors are σ_{inst} are 0.014, 0.013 and 0.024 mag in the respective bands.

The zero-points were adopted as the weighted means on all available local standards on the used image. Their errors were accepted as the errors of these weighted means. For the SAO 1-m telescope, these errors were in the range of 0.010 to 0.018 mag, depending on the band and the night, while for images obtained with the 6m telescope, the uncertainties of zero-points were a factor of 2 smaller. The errors of measured apparent magnitudes for Knots 1–6 were calculated as the sums in quadrature of the Poisson noise standard deviation and the error of zero-points.

We identified the only factor leading to the systematic underestimate of the Knots' fluxes. Depending on the value of seeing β , defined as FWHM of a star profile, a small fraction of a Knot total flux appears lost for photometry with the fixed size aperture. To evaluate this fraction and perform the respective correction, we proceed as follows. We used the HST images obtained in December 2017 (GO program 14716, PI: F. Annibali). We performed the Gaussian filter smoothing by the MIDAS procedure 'filter/gauss' on the HST F606W image to produce images with the seeings β , corresponding to those we had on the images obtained with the ground-based telescopes.

We compare the results of aperture photometry for non-smoothed and smoothed images with the fixed sizes of aperture. From this we evaluate corrections for the measured magnitudes of each Knot with the respective size of aperture, depending on the actual seeing. These corrections are larger for the smaller apertures. They vary from 0.01–0.02 mag for $\beta \sim 1.0$ –1.2 arcsec, to 0.04 mag for $\beta \sim 1.9$ arcsec, to 0.06 mag for β of ~ 2.2 arcsec, and up to 0.07 mag for the few occasional images with β of ~ 2.5 arcsec. These corrections were applied to each magnitude estimate in Tables A1–A6.

3 RESULTS

In Table 4 we briefly summarise results of photometry of all six Knots for the most numerous data, collected for V-band, including their median magnitudes and the estimated amplitudes of variability in this band. The more advanced analysis of the potential variability and the related parameters are presented in Sect. 4.

The resulting lightcurves for all 6 knots in B, V, R bands are combined in Figs. 2 and 3 and discussed in Sect. 5. In Figures 4 to 9, we show the lightcurves of the residual light for each Knot in V-band, that is the observed light minus that of the minimal level. We show these residual lightcurves in three time intervals in order one could better see variations at various time-scales.

In Tables A1–A6 (Appendix A, Sect. A), we present the data on the individual measurements in each band of B, V and R, with the corrections related to the effect of seeing on the loss of light entering the aperture. This issue is described in detail in Sect. 2.6.

4 EXAMINATION OF POSSIBLE VARIABILITY

For Knot 3, outside the time interval of the 'giant eruption' event, discussed in Pustilnik et al. (2017) and Perepelitsyna, Pustilnik (2017), the variability with the amplitude of ~ 0.3 mag is quite evident and does not require special tests. As for the other Knots, the light variations are significantly less pronounced. Therefore, we need to use the known tests to check, whether the observed scatter in the measured magnitudes indicates the real variations, or they are consistent with the scatter due to the adopted observational errors.

As one can see from the data in Tables A1–A6, due to the various reasons, the photometry data in V-band outnumber significantly the results, available for B and R bands, having approximately the similar accuracy. Therefore, it is reasonable to begin the search for possible variability from the dataset of the V-band photometry.

4.1 Methods to search for light variability

Sokolovsky et al. (2017) presented the comparison of various methods to detect photometric variability in time series data in the search for variable stars. We use in the following the two of their methods.

The first one is the well-known χ^2 test. It allows to clearly define, based on the published 'critical' values of χ^2 distribution and the number of observed data, the confidence level, at which the Null hypothesis on the absence of variability can be rejected (assuming that the measured data have Gaussian distribution). Here, statistics χ^2 is $\Sigma(x_i - m_w)^2 / \sigma_i^2$, where σ_i^2 are dispersions of x_i , assumed to have Gaussian distribution and $m_w = \Sigma(x_i / \sigma_i^2) / \Sigma(1 / \sigma_i^2)$ is the weighted mean of x_i .

The second method uses the so-called robust median statistic (RoMS, η) (Enoch et al. 2003; Rose, Hintz 2007). This is defined as $\eta = \Sigma|x_i - \text{median}(x_i)| / \sigma_i$. The reduced RoMS, $\bar{\eta}$ with N–1 degrees of freedom, is defined as follows: $\bar{\eta} = (N-1)^{-1} \times \Sigma|x_i - \text{median}(x_i)| / \sigma_i$.

For this method, there is no published theoretical distribution and respective 'critical' values for various confidence levels. As Enoch et al. (2003) note, if the data x_i represent intrinsically the constant value, the expected value of $\bar{\eta}$ is less than one. The value of $\bar{\eta}$ larger than 1 indicates probable variability. To quantify the likelihood of variability, the authors ran a thousand of Monte Carlo simulations for data samples representing the constant value with the random noise. They adopt the values of $\bar{\eta}_{95}$, $\bar{\eta}_{98}$ and $\bar{\eta}_{99}$, for which 95, 98 and 99 per cent of realisations had $\bar{\eta}$ less than these 'critical' values of $\bar{\eta}$. From their Table 2, it follows that the 'critical' value $\bar{\eta} = 1.2$ was exceeded only in 10 cases of 1000. Hence, one can treat this level of $\bar{\eta}$ as the critical point to reject the Null hypothesis on 'non-variable signal' at the confidence level of $\alpha = 0.01$, or, in the other words, the evidence of detecting variability with probability of $P = 1 - \alpha = 0.99$. The method was further successfully tested on the massive arrays of data by Rose, Hintz (2007) and Burdanov et al. (2014). While for the Gaussian distribution of errors, the RoMS method seems to be less powerful, than χ^2 test (in the sense of the lower confidence probability for

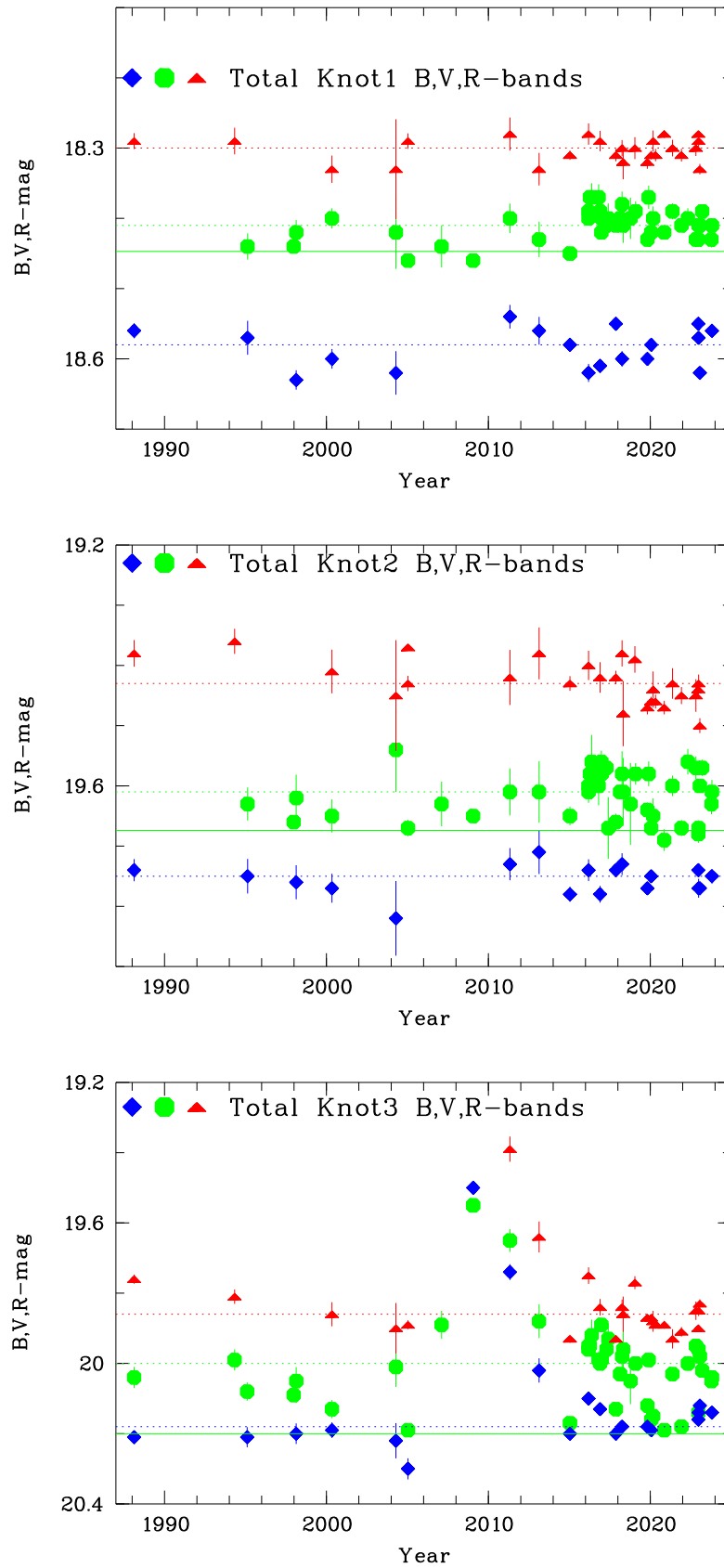


Figure 2. From top to bottom: Lightcurves in B, V, R -bands of Knots 1, 2, 3. Dashed lines show the median magnitudes to help the eye.

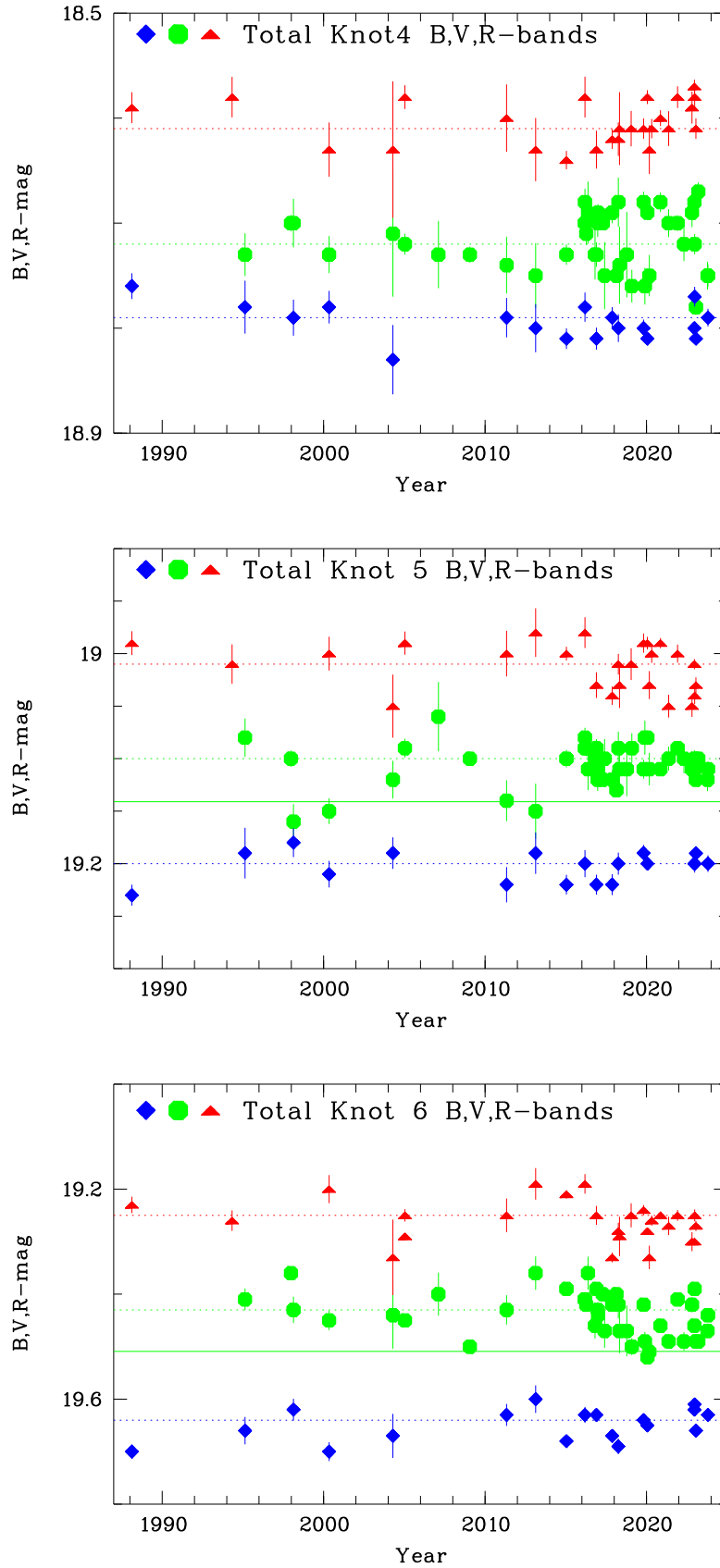


Figure 3. Lightcurves of Knots 4, 5, 6 similar to those in Fig. 2. Dashed lines show the median magnitudes for each band. Solid lines for V show the adopted minimal levels. They are defined to be consistent with the maximal possible number of points at this brightness level.

Table 3. Summary of properties of local standards

SDSS Name (1)	SDSS g, r, i mag (2)	B, V, R mag (3)	$\sigma_g, \sigma_r, \sigma_i$ mag (4)
J095633.91+284953.9	21.08, 20.45, 20.01	21.50, 20.71, 20.23	0.03, 0.03, 0.04
J095635.72+285042.6	20.54, 20.18, 20.16	20.87, 20.32, 20.02	0.03, 0.03, 0.03
J095639.60+285202.4	19.66, 18.21, 17.47	20.34, 18.82, 17.85	0.01, 0.01, 0.01
J095639.81+285207.7	19.09, 17.93, 17.51	19.67, 18.42, 17.62	0.01, 0.01, 0.01
J095643.53+284747.6	18.66, 18.09, 17.84	19.06, 18.33, 17.87	0.01, 0.01, 0.01
J095646.63+284928.3	17.91, 17.22, 16.98	18.36, 17.51, 17.00	0.01, 0.01, 0.01
J095648.62+284854.3	20.81, 19.70, 19.17	21.38, 20.16, 19.40	0.02, 0.02, 0.02
J095649.01+284911.2	20.35, 19.03, 18.24	20.98, 19.58, 18.68	0.02, 0.01, 0.01
J095649.51+285236.6	20.59, 20.34, 20.04	20.90, 20.44, 20.20	0.03, 0.03, 0.04
J095650.57+284950.1	20.66, 19.20, 18.35	21.34, 19.81, 18.83	0.02, 0.01, 0.01
J095652.10+285041.6	21.77, 20.64, 19.07	22.38, 21.12, 20.32	0.05, 0.04, 0.02
J095656.49+284911.7	18.99, 18.64, 18.56	19.33, 18.78, 18.47	0.01, 0.01, 0.01

Table 4. Summary of properties of Knots 1–6

Name (1)	Coord. of Centre J2000 (2)	Aperture diameter (3)	Median V-mag (4)	δV mag (5)
Knot 1	J095646.73+285008.9	10.0"	18.41	~ 0.09
Knot 2	J095646.69+285020.8	8.0"	19.61	~ 0.13
Knot 3*	J095646.25+285023.5	5.0"	20.00	~ 0.30
Knot 4	J095645.60+285015.9	11.0"	18.72	~ 0.11
Knot 5	J095646.15+285009.9	4.4"	19.10	~ 0.08
Knot 6	J095646.78+284954.8	6.0"	19.44	~ 0.16

* δV during the period after the LBV 'giant eruption' event.

a given light curve), this can serve as an independent check of the suspected variability.

4.2 Results of checks of possible variability

In the top part of Table 5, for Knots 1, 2, 4, 5, 6 we present the estimates of χ^2 and the related probability of variability along with the similar data for the reduced RoMS $\bar{\eta}$. Here, the estimates are given for the nominal errors in the Tables with the results of photometry for individual Knots. A brief discussion of the possible effect of the underestimation of the observational errors is presented at the end of this Section.

In Table 5, we present the ranges of the magnitudes m_i (excluding the low-accuracy points on the edges of the range), the weighted mean magnitudes m_w , the weighted mean error $\sigma_w = \sqrt{(N)/\Sigma (1/\sigma_i^2)}$, the weighted rms_w around the weighted mean, and the related value of $\chi^2 = \Sigma(x_i - m_w)^2/\sigma_i^2$, the median of all m_i , and the reduced parameter RoMS, $\bar{\eta} = \Sigma (|m_i - \text{median}|/\sigma_i)/(N-1)$. For all Knots, the number of observations in V-band is $N = 43$.

In the last two columns, we present the probability $P = 1 - \alpha$ for rejection of the Null hypothesis on the non-

variability of the examined samples according to criterion of χ^2 and the value of $\bar{\eta}$. For χ^2 test this is based on the critical points of the χ^2 distribution for the respective values of probability, from Table 2.2a in the book by Bol'shev & Smirnov (1983). As for probabilities, based on the statistics $\bar{\eta}$, we adopt the results of modelling, presented in Enoch et al. (2003).

As one can see in the top part of Table 5, the apparent amplitude of light variations ranges from 0.08 (Knot 5) to 0.16 mag (Knot 6), with the intermediate amplitudes of 0.09, 0.13 and 0.11 mag for Knots 1, 2 and 4. The weighted rms varies between ~ 0.016 and ~ 0.046 mag for various Knots. For the nominal values of the measurement errors, both statistics, χ^2 and $\bar{\eta}$, appear sufficiently large for all 5 Knots, so that the confidence levels α to reject the Null hypothesis, are 0.0005 for χ^2 and 0.01 for $\bar{\eta}$.

While this result looks somewhat surprising, it is worth of commenting the issue of how robust are the conclusions on the variability of the considered Knots. We adopt that the observed light variations reflect the real processes, that is the internal variations plus the noise signal inherent to the measurement methodics. So, the characteristic measure of the significance of variations in both tests, χ^2 and $\bar{\eta}$, is the averaged ratio of the characteristic amplitude of variations to the measurement error.

Therefore, if we, due to the incomplete understanding of the nature of the measurement errors, underestimate them, we get, as a result, the elevated values of both χ^2 and $\bar{\eta}$, and, in turn, the higher confidence levels for detection of variability. In order to check, how the conclusions about the probable variability are conservative, we vary upward all the measurement errors by the factors of 1.41 and 2.0. The former case corresponds roughly to the situation, in which we count the Poisson noise within the Knot aperture twice. We summarise the effect of the underestimated error by a factor of 2.0 in the bottom part of Table 5. For the intermediate factor of 1.41, the probability of variability, based on χ^2 , $P > 0.9995$ for all Knots but Knot 5, for which this is 0.995. Respectively, the probability of variability, based on $\bar{\eta}$ is $P \geq 0.99$ for all Knots but Knot 5, for which it is 0.90.

As one can see, for the underestimation factor of 1.41,

the probability of rejecting the Null hypothesis drops substantially only for Knot 5. For the other four Knots, the variability manifests with the high confidence. Even for the case of the underestimation factor of 2, the results on the variability of Knots 4 and 6 remain robust, for Knot 2, the variability gets less confident, while the variations of light in Knots 1 and 5 appear non significant.

4.3 Lightcurves of the residual components

It is instructive to see the light variations in the analysed Knots at the higher contrast, after the underlying non-variable component light is subtracted. This can give us indications on the variability amplitudes and timescales of the respective objects and to hint the type of the related stars.

For all Knots (apart Knot 3), we estimated the level of the underlying background, taking several points with the minimal brightness and estimating their weighted mean and the scatter around this. The adopted minimal V-band magnitudes are given in the captions of the respective plots in Figures 4–9. These lightcurves are shown in two time intervals (years 1995–2023 and 2015–2023) in order to better distinguish visually variations at the longer and the shorter timescales. The minimal brightness is shown in all light curves as the solid line at $\delta V = 0$. We draw additionally for each plot the dotted line, corresponding to the median magnitude over the whole period.

5 DISCUSSION

5.1 Variability of DDO68-V1

The variability of LBV in DDO68 (DDO68-V1 in Knot 3) was already discussed in many papers, including the variability of spectral features and variations of its optical luminosity (e.g., Pustilnik et al. 2008, 2017; Izotov & Thuan 2009; Perepelitsyna, Pustilnik 2017; Guseva et al. 2022). Its main features are the absence in emission of any metal lines while the observed Balmer lines of Hydrogen and the lines of He I show P Cygni profiles with the typical radial velocities of $\gtrsim 800 \text{ km s}^{-1}$. As for the luminosity variations, this star was caught in the phase of the giant eruption during the years 2008–2011, when its luminosity in V-band approached $M_V \sim -10.6 \text{ mag}$. The total amplitude of its variability was estimated of $\sim 4 \text{ mag}$. Since before the LBV giant eruption, there were no more or less regular observations of this object, our presented monitoring was intended, in particular, to examine the behaviour of the LBV light curve after such an event.

The spectral monitoring of Knot 3 in 12 epochs during years 2008–2018 was presented recently by Guseva et al. (2022). In particular, they discovered variations of the LBV broad H α -line flux by a factor of a thousand during their decade-long observations. The two latest their measurements, in April 2016 and April 2018, are obtained within several days from our imaging observations. In April 2016, the flux of the broad H α -line was 20 times lower than its maximal value near the peak of the 'giant eruption', while in April 2018 it was below the detection level, that is at least several times smaller. Our light curve of Knot 3 at these epochs (see Table A3 and Figure 6), is consistent with the

fall of the LBV light after the giant eruption to the deep minimum in 2015, with the subsequent episodic maxima mimicking the S Dor phase variations. The latter spectral observations of the LBV appear close to these local maxima. The behaviour of the broad H α -line flux indicates that this is the tracer of the strongly decaying 'giant eruption' shell. We postpone the description and analysis of the Knot 3 data and the derived light curves for DDO68-V1 to the forthcoming dedicated paper.

5.2 Variability of the other star-forming regions

We use all available DDO68 images to check the potential of the integrated photometry of the most metal-poor SF regions to search for new variable supergiants with the lowest known metallicities. This variant was suggested in the paper of Pustilnik et al. (2017) for the ground-based telescopes situated in observatories with the superb seeings. Of course, the better seeing in images of this kind monitoring programs, the simpler one can separate individual variable supergiants. In fact, our results described below, suggest that this task can be partly accomplished with more relaxed conditions if the accuracy of photometry, the cadence period and the time span of monitoring are optimised for the expected parameters of the searched variability.

For Knot 1, the results of our statistical tests are indicative on its V-band variations in the range 18.37–18.46 mag, with the median of $V_{\text{Kn.1,med}} = 18.41$. As one can see in Table 5, the detection of variability is confident, but somewhat less robust with respect of the (potentially) underestimated measurement errors in comparison to Knots 6, 4 and 2. We conduct the preliminary consideration of possible stars that can be responsible for the observed amplitude of light variations of $\delta V_{\text{Kn.1}} \sim 0.09 \text{ mag}$. The two brightest stars of this region, No. 13 and No. 18 according to the list in Pustilnik et al. (2017), are blue supergiants (BSG) with the measured on May 2, 2010 V-band magnitudes of 23.81 and 24.13 mag, and the colour ($V-I$) = -0.09 and -0.21 mag , respectively. The corresponding absolute magnitudes are $M_V = -6.77$ and -6.45 mag . The V-band light of star No. 13 is $\sim 5.4 \text{ mag}$ fainter than the total light of Knot 1, that is comprises only 0.7 per cent of this. The star No. 18 contributes to the total V-band light of Knot 1 only 0.5 per cent. The observed light variations of Knot 1 imply very strong variations in one or both of these two blue supergiants: $\delta V_{\text{No.13}} \sim 3.0 \text{ mag}$, and $\delta V_{\text{No.18}} \sim 3.3 \text{ mag}$.

Such large amplitudes are quite atypical for blue supergiants. Even LBVs during the so-called S Dor stage (normal eruptions) show amplitudes at the time-scale of years of up to 2.5 mag (e.g. van Genderen 2001). Only for a few observed Milky Way LBVs, such as $\eta \text{ Car}$, P Cyg and a number of extragalactic LBVs, such as NGC 2363-V1 (Petit, Drissen & Crowther 2006), LMC R127 (Walborn et al. 2008) and UGC2773-OT (Smith et al. 2016), the so-called 'giant eruptions' are registered, with the amplitudes of four and more magnitudes. Similarly, the large amplitude events are observed for a number of the so-called Supernova impostors. However, their relation to a certain type of massive stars is not yet clear.

As for the data on the S Dor phase amplitudes up to $\sim 2.5 \text{ mag}$, they all are picked up on the sample of relatively metal-rich LBVs in the Milky Way, Magellanic Clouds, M31

Table 5. Statistical parameters of variability for Knots 1, 2, 4, 5, 6

Name	V range mag	$V_{\text{mean,w}}$ mag	σ_w mag	rms_w mag	χ^2	V_{med} mag	$\bar{\eta}$	Prob. var. on χ^2	Prob. var. on $\bar{\eta}$
(1)	(2)	(3)	(4)	(5)	(6)	(7)	(8)	(9)	(10)
For case of the nominal errors.									
Knot 1	18.37-18.46	18.413	0.009	0.021	229	18.41	1.70	>0.9995	>0.99
Knot 2	19.56-19.69	19.622	0.016	0.040	270	19.61	2.02	>0.9995	>0.99
Knot 4	18.67-18.78	18.713	0.012	0.029	290	18.72	2.05	>0.9995	>0.99
Knot 5	19.08-19.16	19.103	0.009	0.016	151	19.10	1.47	>0.9995	>0.99
Knot 6	19.36-19.52	19.441	0.012	0.046	641	19.44	2.85	>0.9995	>0.99
For case of errors larger than nominal by a factor of 2.0.									
Knot 1	18.37-18.46	18.413	0.009	0.021	57	18.41	0.85	0.90	...
Knot 2	19.56-19.69	19.622	0.016	0.040	67	19.61	1.01	0.99	0.90
Knot 4	18.67-18.78	18.713	0.012	0.029	72	18.72	1.03	0.995	0.90
Knot 5	19.08-19.16	19.103	0.009	0.016	38	19.10	0.74
Knot 6	19.36-19.52	19.441	0.012	0.046	160	19.44	1.43	>0.9995	>0.99

Col. 2: full range of variations in V band; Col. 3: weighted mean V-mag; Col. 4: weighted mean error $\sqrt{(N)/\Sigma (1/\sigma_i^2)}$; Col. 5: weighted rms about the weighted mean; Col. 6: Value of χ^2 ; Col. 7: median V-mag; Col. 8: value of parameter $\bar{\eta}$; Col. 9: Probability of 'variability', $P = 1 - \alpha$, based on χ^2 ; Col.10: similar probability, based on $\bar{\eta}$. See Sect. 4 and 5.2. For all Knots, $N_{\text{obs}} = 43$.

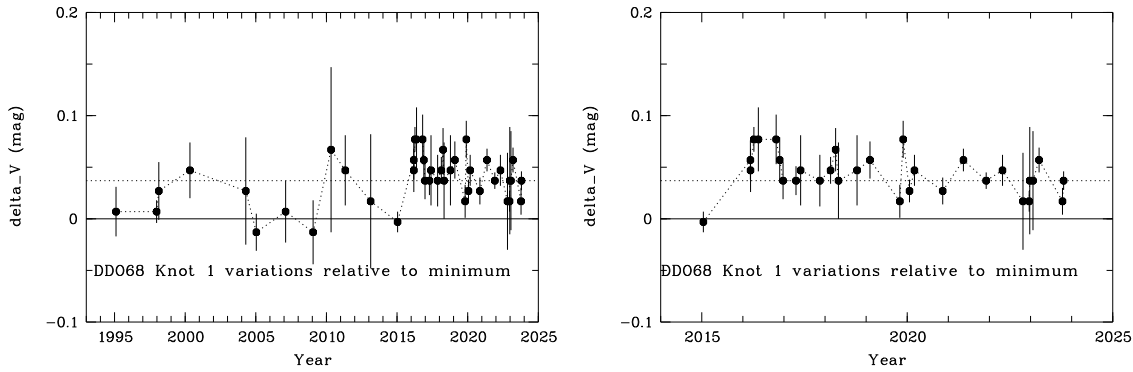


Figure 4. Light curves of 'variable' component of Knot 1 (relative to its minimal brightness of $V=18.447$ mag) in V-band in two time intervals: 1995–2023 and 2015–2023.

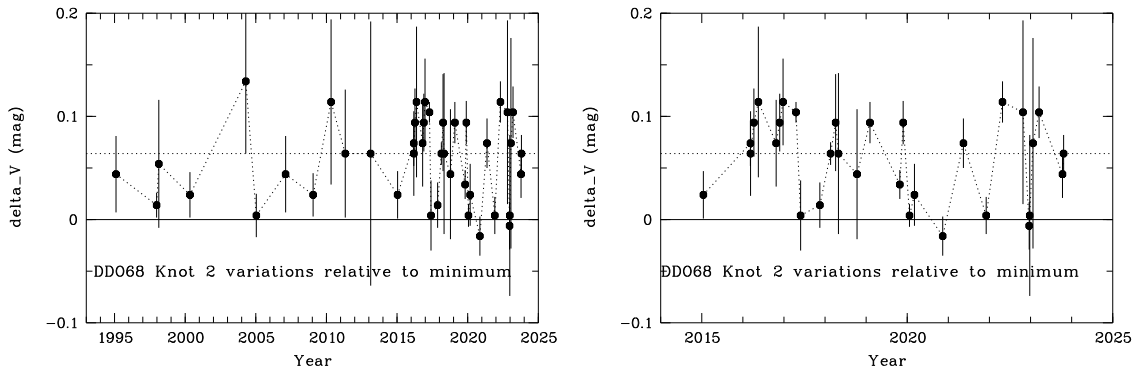


Figure 5. Light curves of 'variable' component of Knot 2 (relative to its minimal brightness of $V=19.674$ mag) in V-band in two time intervals: 1995–2023 and 2015–2023.

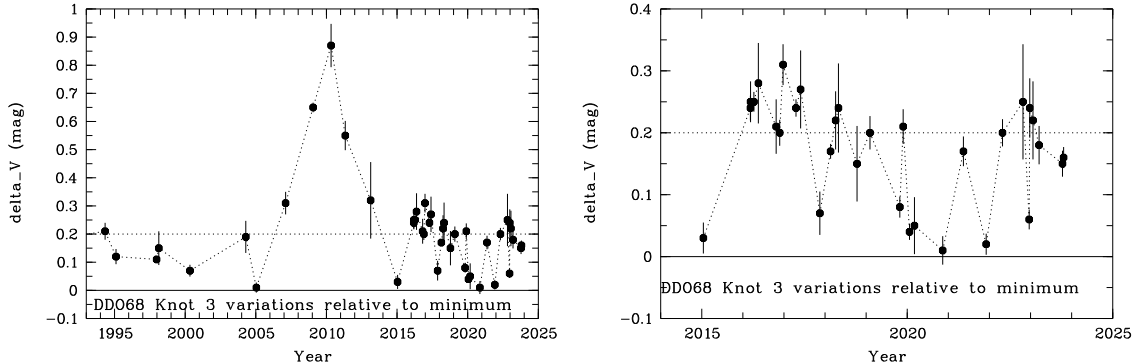


Figure 6. Light curves of 'variable' component of Knot 3 (relative to its minimal brightness of $V=20.20$ mag) in V-band in two time intervals: 1995-2023 and 2015-2023.

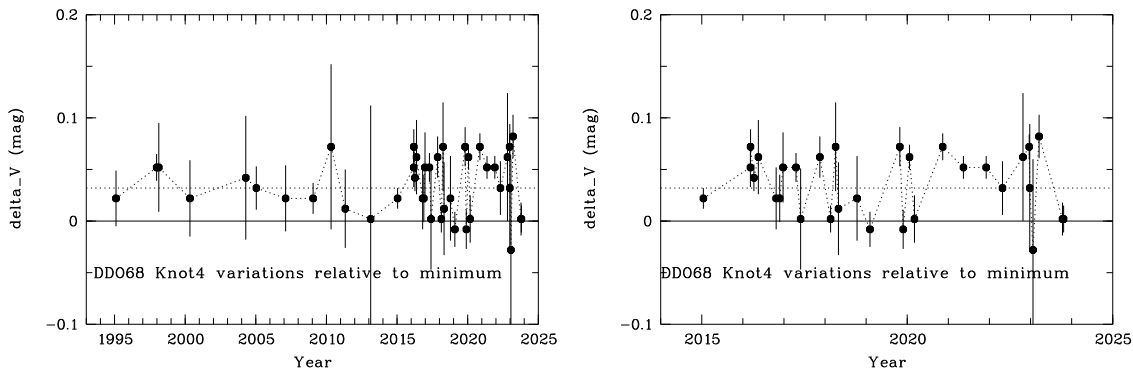


Figure 7. Light curves of 'variable' component of Knot 4 (relative to its minimal brightness of $V=18.775$ mag) in V-band in two time intervals: 1995-2023 and 2015-2023.

and other 'metal-rich' galaxies. Therefore, they can be not representative of LBVs in the XMP regime.

In fact, the S Dor phase amplitudes may depend on the LBV metallicity. The example of DDO68-V1 directly indicates to this possibility. Of course, the single unique case of variability of DDO68-V1 does not pretend to have statistical implications. However, the precedent of its S Dor variations with the amplitude of up to 3.5 mag, discovered in our forthcoming paper, gives the clear hints on the probable larger S Dor type variations in the XMP LBVs. However, to be confident that these variations are consistent with the typical S Dor behaviour, that is of almost constant bolometric luminosity and the related changes of colours versus the luminosity (e.g., Solovyeva et al. 2019), it takes to analyse the multi-colour data for a wide range of DDO68-V1 light variations.

Finally, we should comment on two rather bright non star-like objects near the center of Knot 1, with $V \sim 21.3$ – 21.5 mag. These can be compact HII regions, excited by the hot massive stars. Their contribution to the total light of Knot 1 can be an order of magnitude larger than that of the mentioned above BSGs (No. 13 and 18). Hence, their required amplitudes of variability will be of less than ~ 1 mag. However, such objects are too luminous for O-stars at the main sequence. Hence, one expects that these HII regions are excited by a 'cluster' of massive stars. Therefore, they

are less probable contributors to the observed variability of Knot 1.

For Knot 2, the available data in V-band indicate the range of variations from 19.69 to 19.56 mag. Hence, one can suspect variability with the amplitudes of ~ 0.13 mag. The R-band data are much more sparse, but indicate the similar amplitude of ~ 0.10 mag, from 19.46 to 19.36 mag. The B-band lightcurve is even more sparse, and due to the larger errors in the extremums, there is no indication on the real variations larger than 0.05 mag. The two brightest stars of this region are the blue supergiant No. 19 with $V = 24.13$ mag and $(V-I) = -0.21$ mag, as on the epoch of the HST image (2010.05.02), and the red supergiant No. 29 with $V = 24.36$ mag and $(V-I) = 1.41$ mag. They contribute, respectively, 1.5 and 1.2 per cent of the total V-band light of Knot 2. To produce the visible variations of 0.13 mag, these stars should vary with the amplitude of ~ 2.4 – 2.6 mag.

For Knot 4, the variations in V-band (18.67 to 18.78) indicate the amplitude of $\delta V \sim 0.11$ mag. There are about 10 blue and red supergiants within Knot 4, with V-mag from 23.00 to 24.40 mag. They contribute to the integrated light of Knot 4 from ~ 1.8 down to ~ 0.3 per cent. Therefore, for variations with the amplitude of ~ 0.11 mag, the individual stars should vary by a factor of 5 (1.8 mag) to 30 (3.7 mag). With that large number of candidate strongly variable supergiants, more data of high accuracy is necessary for indi-

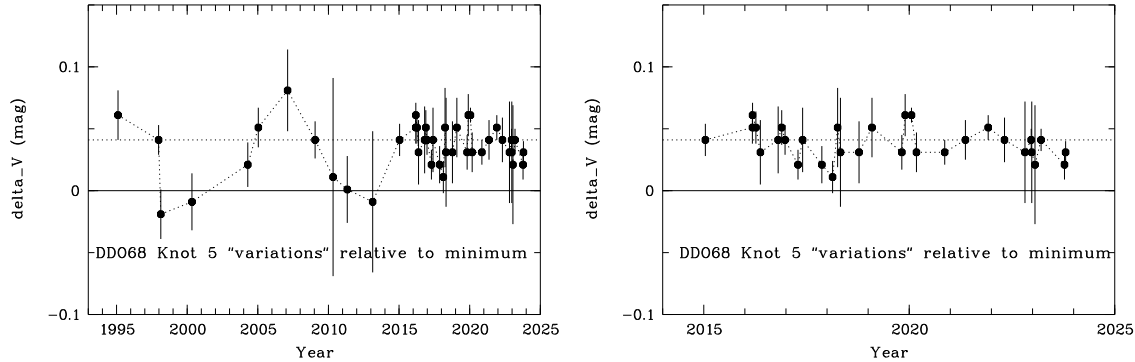


Figure 8. Light curves of 'variable' component of Knot 5 (relative to its minimal brightness of $V=19.141$ mag) in V-band in two time intervals: 1995-2023 and 2015-2023.

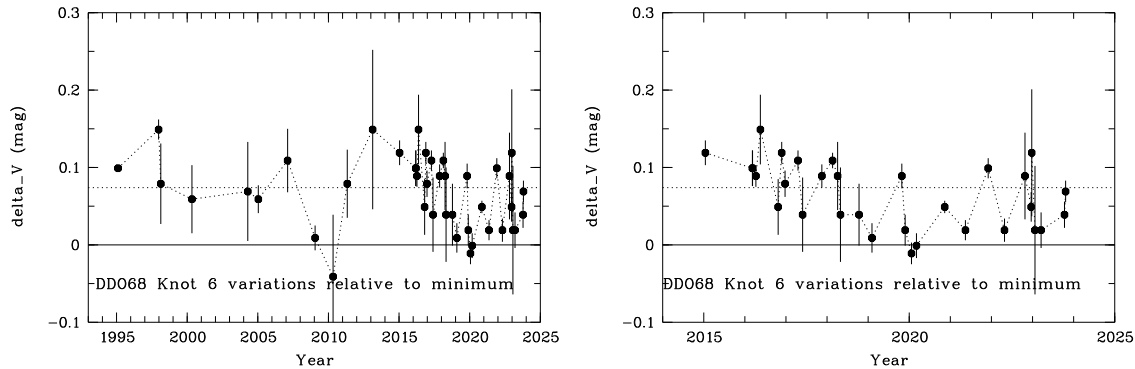


Figure 9. Light curves of 'variable' component of Knot 6 (relative to its minimal brightness of $V=19.509$ mag) in V-band in three time intervals: 1995-2023 and 2015-2023.

vidual stars on the images of HST to try to assign the visible variations of Knot 4 to a specific star or stars.

For Knot 5, the amplitude of V-band light variations does not exceed 0.08 mag. Apart the young cluster itself, three nearby individual supergiant stars fall into the used aperture, No. 7, 21 and 42, with V-band magnitudes of 23.3 to 24.5 mag. They contribute to the total light within the used aperture from ~ 3.5 to ~ 1 per cent. Therefore, the visible light variations in Knot 5 require either variations of nearby stars by a factor of 2.5–8, or substantial variations of massive stars inside the cluster.

For Knot 6, the V-band variations are the most prominent, with the full range of 19.36 to 19.52 mag. We also do see partly correlated variations in V and B bands over the whole period of ~ 18 years. Variations in R-band, despite the data are significantly more sparse, also look like to occur in phase with those in V-band. In Fig. 3 (bottom panel), showing all three B, V, R lightcurves for Knot 6, we draw by the dotted lines the median values for each band. We also draw by the solid line the estimated level of the minimal light in V band.

This allows us to estimate the full range of variations in V, B and R bands of ~ 0.16 , ~ 0.10 , ~ 0.10 mag, respectively. We first suggest that the observed variability of Knot 6 is related to the light variations of its brightest supergiant, identified as star No. 2 in the DDO68 list of the most luminous stars related to the star-forming regions with the

lowest gas O/H (Pustilnik et al. 2017). This candidate Yellow (warm) Hypergiant (e.g. Humphreys et al. 2013), with the HST-based $V = 21.47$ mag and $M_V = -9.11$ mag, is the second most luminous star after DDO68-V1 at that epoch (see Fig. 6 in Pustilnik et al. (2017)).

At the HST image, the V-band light of this star comprises $\sim 20.5\%$ of the rest Knot 6 light within the aperture with diameter of 6 arcsec. The brightness increase by $\delta V = 0.16$ mag in the total light of Knot 6 corresponds to the brightening of star No. 2 by 0.7 mag, reaching the absolute magnitude of $M_V \sim -9.8$. According to its HST colour ($V-I$) = 0.33 mag, this luminous star is currently classified as Yellow Hypergiant (YHG). While LBV stars spend most of their life time as blue, their evolutionary tracks also reach the area of Yellow Hypergiants, so one can find them occasionally in this phase (e.g. van Genderen 2001).

Besides, one can not exclude that its colour is affected by a circumstellar envelope, often observed near evolved massive stars (e.g. van Genderen 2001; Kniazev, Gvaramadze, Berdnikov 2017). So that, with the account of dereddening, it can be bluer and belong to A, or even to B hypergiants. Probably, the medium resolution spectroscopy of this star, with the expected V-magnitude between 21.47 and ~ 20.9 mag, will help to better determine its spectral class.

One can also consider an alternative case, when the observed variability of Knot 6 is related to variability of

the fainter blue supergiant, the star No. 11, with $M_V = -7.11$ mag, and $(V-I) = -0.11$. Its V-band magnitude of 23.42 mag, corresponds to ~ 2.5 per cent of the integrated light of Knot 6. The other brightest stars situated around Knot 6, No. 4, 10 and 17, are situated far outside the aperture with the diameter of 6 arcsec, used to monitor the HII region potential variability. To produce the variations of the knot integrated light with the amplitudes of 0.16 mag, this star should brighten by ~ 7 times, or by ~ 2.1 mag, reaching $M_V \sim -8.2$ mag. Thus, one can think on this B-supergiant as a one more LBV candidate in the phase of S Dor-type variability.

From the examination of the lightcurves and tables with photometric data for the individual DDO68 Knots, one can estimate the typical time scale of the significant variability (peak-to-peak) in the Knots where the statistical analysis indicates a sufficiently high probability of the real variations. These time scales can be useful for a more detailed analysis.

In particular, for the strongest (after Knot 3) variability in Knot 6, one can see the minima of the V-band light near epochs of 2009.1, 2020.0 and 2023.2, while the maximal brightness was reached near epochs of 1998.0, 2015.0–2016.3. That is the typical long-term variability of a star in this Knot has the characteristic times of 2–5 years from bottom to top and back. This is important to have in mind when checking the potential variability of the luminous stars at the shorter timescales on the images available in the HST archive. So, the estimated amplitudes of the brightest stars in these regions, of ~ 0.7 –3 mag on the timescales of ~ 2 years, will appear as only 0.03–0.12 mag variation on the timescale of 1 month.

The above analysis and discussion of the integrated light variations for various SF regions in DDO68, implies that the detected amplitudes of 0.08–0.16 mag correspond to the brightening of their brightest supergiants from the apparent $V \sim 23$ –24 mag (or $V \sim 21.5$ mag for the YHG in Knot 6) to the levels of $V \sim 20.5$ –21.5 mag. The stellar objects of such magnitudes are accessible for the medium resolution spectroscopy with the ground-based large telescopes. While their light contribution to the whole emission of the associated HII-region comprises at most 10–15 per cent, for the properly positioned long slit with the width of $\lesssim 1$ arcsec, its contrast can increase several times. Thus, the practical recommendation for the continuation of monitoring of the 'Northern Ring' includes the spectral follow-up of the regions, in which one detects the bright phase of the lightcurve. This will allow us to pick-up the preliminary information on the spectral properties of the most metal-poor supergiants/hypergiants in their bright phases.

6 SUMMARY

We summarise the presented results and the discussion above and draw the following conclusions:

(i) The unique LBV DDO68-V1 was discovered in January 2008 in the void galaxy DDO68 near the center of HII-region 'Knot 3' with the almost record-low metallicity [$12 + \log(O/H) \sim 7.1$ dex]. The previous sparse lightcurve of Knot 3 for the period of 2005–2015, when the LBV 'giant eruption' was discovered, was presented by Pustilnik et al. (2017). Here we extend the lightcurve of Knot 3, adding our

photometry with 3 telescopes for 35 epochs till the end of 2023. We also use the archive data from 10 other telescopes. The light variations of Knot 3 with the amplitude of up to ~ 0.3 mag during the last 8 years are well documented. The lightcurve for the LBV itself and its discussion will be presented in the forthcoming paper.

(ii) Apart Knot 3, our images cover five more SF regions (Knots) in or near the so-called DDO68 'Northern Ring'. There are many various supergiant stars in these Knots, listed in Pustilnik et al. (2017), which can, in principle, show large light variations. Such supergiant variability would manifest it as 'small' variations in the total light of these Knots. We perform the photometry of these Knots, similar to that of Knot 3, and conduct the statistical analysis of the respective data sets to check whether they are consistent with the Null hypothesis on their non-variability.

(iii) With the use of the well-known criterion χ^2 and the additional statistics RoMS, the Null hypothesis is rejected at the confidence level of $\alpha = 0.0005$ (for χ^2) for Knots 1, 2, 4, 5, 6. Their peak-to-peak amplitudes are of $\delta V \sim 0.09, 0.13, 0.11, 0.08$ and 0.16 mag, respectively.

(iv) The detected variations of Knots' light are naturally explained as manifestations of variability in the brightest supergiants within these SF regions. Since the contribution of individual supergiants to the integrated light of their Knots comprises of $\lesssim 1$ –10 per cent, the related variations of the supergiants should reach amplitudes of $\delta V \sim 0.7$ –3.5 mag. With so strong variations, one can expect to detect the additional LBV candidates in these Knots. In Knot 6, if the light variations are related to those of the candidate warm hypergiant, their amplitude can be only ~ 0.7 mag.

ACKNOWLEDGEMENTS

The authors are grateful to A. Valeev for help with BTA observations, to L. van Zee, D. Hunter, B. Elmegreen, U. Hopp, L. Makarova, R. Swaters, B. Mendéz, V. Taylor, R. Jansen, R.A. Windhost, S.C. Odewan, J.E. Hibbard for providing archival CCD images of DDO68, obtained for their observational programs. We are pleased to thank P. Kaigorodov and D. Kolomeitsev for their kind help in extracting the data from archive tapes. The authors thank the anonymous referee for careful reading the manuscript and for valuable comments, which helped us to improve the paper content. The work was performed as part of the SAO RAS government contract approved by the Ministry of Science and Higher Education of the Russian Federation. Observations at the 6-m telescope BTA are supported by funding from the Ministry of Science and Higher Education of the Russian Federation. (agreement No 14.619.21.0004, project identification RFMEFI61914X0004). EES acknowledges partial support from M.V.Lomonosov Moscow State University Program of Development. We acknowledge the use of the SDSS database. Funding for the Sloan Digital Sky Survey (SDSS) has been provided by the Alfred P. Sloan Foundation, the Participating Institutions, the National Aeronautics and Space Administration, the National Science Foundation, the U.S. Department of Energy, the Japanese Monbukagakusho, and the Max Planck Society. The SDSS Web site is <http://www.sdss.org/>. The SDSS is managed by the Astrophysical Research Consortium (ARC)

for the Participating Institutions. This research is based on observations made with the NASA/ESA Hubble Space Telescope obtained from the Space Telescope Science Institute, which is operated by the Association of Universities for Research in Astronomy, Inc., under NASA contract NAS 5-26555. These observations are associated with program ID GO 11578 (PI A.Aloisi).

7 DATA AVAILABILITY

All discussed photometric data for Knots 1–6 are contained in Tables A1 – A6 in the Supplementary material in the electronic form.

REFERENCES

- Abazajian K.N., Adelman-McCarthy J.K., Agüeros M.A. et al., 2009, *ApJS*, 182, 543
- Afanasiev V.L., & Moiseev A.V., 2005, *Astron. Lett.* 31, 193
- Annibali F., La Torre V., Tosi M., et al., 2019, *MNRAS*, 482, 3892
- Barkana R. & Loeb A., 2001, *Phys. Reports*, 349, 125 (arXiv:astro-ph/0010468)
- Berg D.A., Skillman E.D., Marble A., et al. 2012, *ApJ*, 754, 98
- Bol’shev L.N., Smirnov N.V., *Tables of Mathematical Statistics*, 1983, Nauka Publishers, Moscow (in Russian)
- Burdanov A.Y., Krushinsky V.V., Popov A.A. 2014, *Astrophysical Bulletin*, 69, 368
- Cannon J.M., Johnson M., McQuinn K.B.W., et al., 2014, *ApJ Lett.*, 787, 1
- Chen Y., Bressan A., Girardi L., Marigo P., Kong X., Lanza A., 2015, *MNRAS*, 452, 1068
- Cook D.O., Dale D.A., Johnson B.D., van Zee L., et al., 2014, *MNRAS*, 445, 881
- Eldridge J.J., Stanway E.E., 2022, *ARAA*, 60, 455
- Enoch M.L., Brown M.E., Burgasser A.J., 2003, *AJ*, 126, 1006
- Garcia M., Evans C.J., Bestenlehner J.M. et al., 2021, *Experimental Astronomy*, 51:887-911
- Gull M., Weisz D.R., Senchyna P., et al., 2022, *ApJ*, 941, 206
- Guseva N.G., Izotov Y.I., Thuan T.X., 2000, *ApJ*, v.531, p.776
- Guseva N.G., Thuan T.X., Izotov Y.I., 2022, *MNRAS*, v.512, I.3, pp.4298-4307
- Hirschauer A., Crouzet N., Habel N., et al. 2024, *AJ*, 168, 23
- Hopp U. & Schulte-Ladbeck R.E., 1995, *A&A Suppl.Ser.*, 111, 527
- Humphreys R.M., & Davidson K., 1994, *PASP*, 106, 1025
- Humphreys R.M., Davidson K., Grammer S., Kneeland N., Martin J.C., Weis K., Burggraf B., 2013, *ApJ*, 773, 46
- Hunter D.A., & Elmegreen B.G., 2006, *ApJ Suppl.Ser.* 162, 49
- Izotov Y.I., Foltz Craig B., Green R. F., Guseva N. G., Thuan T. X., 1997, *ApJ*, 487, L37
- Izotov Y.I., Thuan T.X., 2007, *ApJ*, 665, 1115
- Izotov Y.I., Thuan T.X., 2009, *ApJ*, 690, 1797
- Kniazev A.Y., Pustilnik S.A., in Whitelock P., Dennefeld M., Leibundgut B. eds. *The Scientific Requirements for Extremely Large Telescopes*, Proc. of IAU Symp. 232, Cambridge, Cambridge University Press, 2006, pp.306-307
- Kniazev A.Y., Gvaramadze V.V., Berdnikov L.N., in: "Stars: From Collapse to Collapse", Proc. of a conference held at Special Astrophysical Observatory, Nizhny Arkhyz, Russia 3-7 October 2016. Edited by Yu.Yu. Balega, D.O. Kudryavtsev, I.I. Romanyuk, and I.A. Yakunin. San Francisco: Astronomical Society of the Pacific, 2017, v.510, p.480
- Leitherer C., Schaerer D., Goldader J.D., et al., 1999, *ApJS*, 123, 3
- Legrand F., Kunth D., Roy J.-R., Mas-Hesse J. M., Walsh J. R., 1997, *A&A*, 326, L17
- Lorenzo M., Garcia M., Najarro F., Herrero A., Cerviño M., Castro N., 2022, *MNRAS*, 516, 4164
- Lupton R., et al. 2005, <http://www.sdss.org/dr5/algorithms/sdssUBVRITR>
- Makarov D.I., Makarova L.N., Pustilnik S.A., Borisov S.B., 2017, *MNRAS*, 466, 556
- Makarova L.N., & Karachentsev I.D., 1998, *A&A Suppl.Ser.*, 133, 181
- Martins F., Palacios A., 2021, *A&A*, 645, id.A67
- Maseda M.V., Lewis Z., Matthee J., et al., 2023, *ApJ*, 956, id. 11
- Mendez B., Davis M., Moustakas J., Newman J., Madore B.F., Freedman W.L., 2002, *AJ*, 124, 213
- Perepelitsyna Y.A., Pustilnik S.A., in: Proc. of SAO inter. conference "Stars: From Collapse to Collapse", Nizhny Arkhyz, Oct.3-7, 2016. Edited by Yu.Yu. Balega, D.O. Kudryavtsev, I.I. Romanyuk, and I.A. Yakunin. 2017, *ASP Conf. Series*, 510, 484
- Petit V., Drissen L., Crowther P.A., 2006, *AJ*, 132, 1756
- Petrov B., Vink J.S., Gräfener G., 2016, *MNRAS*, 458, 1999
- Pustilnik S.A., Kniazev A.Y., Pramskij A.G., 2005, *A&A*, 443, 91
- Pustilnik S.A., Tepliakova A.L., Kniazev A.Y., Burenkov A.N., 2008, *MNRAS Lett.*, 388, L24
- Pustilnik S.A., Makarova L.N., Perepelitsyna Y.A., Moiseev A.V., Makarov D.I., 2017, *MNRAS*, 465, 4985
- Pustilnik S.A., Perepelitsyna Y.A., Kniazev A.Y., 2016, *MNRAS*, 463, 670
- Pustilnik S.A., Kniazev A.Y., Perepelitsyna Y.A., Egorova E.S., 2020, *MNRAS*, 493, 830
- Pustilnik S.A., Egorova E.S., Kniazev A.Y., Perepelitsyna Y.A., Tepliakova A.L., Burenkov A.N., Oparin D.V., 2021, *MNRAS*, 507, 494
- Pustilnik S.A., Kniazev A.Y., Tepliakova A.L., Perepelitsyna Y.A., Egorova E.S., 2024, *MNRAS*, 527, 11066
- Rose M.B. & Hintz E.G., 2007, *AJ*, 134, 2067
- Sanyal D., Langer N., Szecsi D., Yoon S.-C., Grassitelli L., 2017, *A&A*, 597, A71
- Schootemeijer A., Lennon D.J., Garcia M., Langer N., Hastings B., Schürmann C., 2022, *A&A*, 667, id. A100
- Shatsky N., Belinski A., Dodin A., et al., in "Ground-Based Astronomy in Russia. 21st Century", Proceedings of the All-Russian Conference held 21-25 September, 2020 in Nizhny Arkhyz, Russia. Edited by I.I. Romanyuk, I.A. Yakunin, A.F. Valeev, D.O. Kudryavtsev, 2020, p. 127-132 (arXiv:2010.10850)
- Skillman E., Salzer J.J., Berg D.A., et al., 2013, *AJ*, 146, 3

- Smith N., & Owocki S.P., 2006, ApJ, 645, L45
- Smith N., 2014, ARAA, 52, 487 Mass Loss: Its Effect on the Evolution and Fate of High-Mass Stars
- Smith N., Andrews J.E., Mauerhan J.C., Zheng W.K., Filippenko A.V., Graham M.L., Milne P., 2016, MNRAS, 455, 3546
- Sokolovsky K.V., Gavras P., Karamelas A., et al., 2017, MNRAS, 464, 274
- Solovyeva Y., Vinokurov A., Fabrika S., et al., 2019, MNRAS, 484, L24-L28
- Swaters R.A., & Balcells M., 2002, A&A, 390, 863
- Szesci D., Langer N., Yoon S.-C., Debashis S., de Mink S., Evans C.J., Dermine T., 2015, A&A, 581, A15
- Taylor V.A., Jansen R.A., Windhorst R.A., Odewan S.C., Hibbard J.E., 2005, ApJ, 630, 784
- Telford O.G., McGuinn K.B.W., Chisholm J., Berg D.A., 2023, ApJ, 943:65 (17pp)
- van Genderen A.M., 2001, A&A, 366, 508
- Vink J.S., 2022, Annu. Rev. Astron. Astrophys., 60, 203
- Walborn N., Stahl O., Carmen R., et al., 2008, ApJ, 683, L33

This paper has been typeset from a \LaTeX file prepared by the author.

APPENDIX A: SUPPLEMENTARY MATERIALS

In Tables A1 – A6 we present all results of integrated photometry in B, V and R-bands for the DDO68 star-forming regions Knots 1–6, located in the so-called 'Northern Ring' or nearby (Knot 6). The presented magnitudes include the upward corrections of the measured light which account the loss of the light in the fixed-size aperture for different seeing, as explained in the end of Sect. 2.6. The date in the first column is given in the formate YYYYMMDD. Abbreviations in column Ref. Notes are as follows: CA3.5 - 3.5m telescope of Calar Alto Observatory, Spain; INT - Isaac Newton Telescope at Canary Icelands, NOT - Nordic Optical Telescope at Canary Icelands, KeckII - Keck II 10m telescope at Mauna Kea, Hawaii; KPNO 4m - Kitt Peak National Observatory 4m telescope, Arizona, USA; VATT - Vatican 1.8m telescope at Mt.Graham International Observatory, Arizona, USA; SDSS - Apache Point Observatory 2.5m telescope, New Mexico, USA; SAO BTA - the 6m telescope of Special Astrophysical Observatory, Russia; KP2.1 - Kitt Peak National Observatory 2.1m telescope, Arizona, USA. V-band magnitudes were adopted from g-filter magnitude and the colour $V-g$, measured in these Knots for the similar brightness; HST - 2.6m Hubble Space Telescope; SAO 1m - 1m telescope of Special Astrophysical Observatory, Russia; CMO 2.5m - 2.5m telescope of Caucasian Mountain Observatory of Moscow State University, Russia.

Table A1. Summary of our B, V, R total magnitude estimates for DDO68 star-forming region Knot 1

Date	B	σ_B	V	σ_V	R	σ_R	Ref. Notes
19880214	18.56	0.011	–	–	18.29	0.011	CA3.5
19940502	–	–	–	–	18.29	0.019	INT 2.54m
19950207	18.57	0.024	18.44	0.019	–	–	NOT 2.56m
19971223	–	–	18.44	0.007	–	–	KeckII
19980217	18.63	0.014	18.42	0.018	–	–	KPNO 4m
20000503	18.60	0.014	18.40	0.014	18.33	0.019	VATT 1.8m
20040416	18.62	0.031	18.42	0.052	18.33	0.071	SDSS
20050112	–	–	18.46	0.009	18.29	0.011	SAO BTA
20070209	–	–	18.44	0.030	–	–	KP2.1 interp. from $V - g$
20090121	–	–	18.46	0.007	–	–	SAO BTA
20100502	–	–	18.38	0.080	–	–	HST
20110305	18.54	0.017	18.40	0.021	18.28	0.024	KPNO 0.9m
20130217	18.56	0.020	18.43	0.025	18.33	0.023	KPNO 0.9m
20150114	18.58	0.009	18.45	0.008	18.31	0.007	SAO BTA
20160307	–	–	18.39	0.008	–	–	SAO 1m
20160308	18.62	0.013	18.40	0.009	18.28	0.015	SAO 1m
20160407	–	–	18.37	0.008	–	–	SAO 1m
20160517	–	–	18.37	0.020	–	–	SAO 1m
20161022	–	–	18.37	0.018	–	–	SAO 1m
20161124	18.61	0.010	18.39	0.009	18.29	0.015	SAO 1m
20161224	–	–	18.42	0.010	–	–	SAO 1m
20161231	–	–	18.40	0.007	–	–	SAO 1m
20170418	–	–	18.41	0.006	–	–	CMO 2.5m
20170529	–	–	18.40	0.021	–	–	SAO 1m
20171116	18.55	0.010	18.41	0.009	18.31	0.009	SAO BTA
20180219	–	–	18.40	0.006	–	–	CMO 2.5m
20180405	18.60	0.011	18.38	0.018	18.30	0.011	SAO 1m
20180430	–	–	18.41	0.025	18.32	0.024	SAO 1m
20181011	–	–	18.40	0.029	–	–	SAO 1m
20190118	–	–	–	–	18.30	0.016	CMO 2.5m
20190203	–	–	18.39	0.014	–	–	SAO 1m
20191026	18.60	0.008	18.43	0.009	18.32	0.009	SAO BTA
20191125	–	–	18.37	0.017	–	–	SAO 1m
20200119	–	–	–	–	18.31	0.006	SAO BTA
20200120	18.58	0.006	18.42	0.005	–	–	SAO BTA
20200304	–	–	18.40	0.017	18.29	0.015	SAO 1m
20200426	–	–	–	–	18.31	0.009	SAO BTA
20201111	–	–	18.42	0.007	18.28	0.006	SAO BTA
20210514	–	–	18.39	0.011	–	–	SAO 1m
20210516	–	–	–	–	18.30	0.012	SAO 1m
20211202	–	–	18.41	0.006	18.31	0.009	SAO BTA
20220426	–	–	18.40	0.014	–	–	SAO 1m
20221025	–	–	18.43	0.011	18.30	0.011	SAO 1m
20221220	18.55	0.005	18.43	0.008	18.28	0.005	SAO BTA
20221225	18.57	0.008	18.41	0.008	18.29	0.009	SAO 1m
20230123	18.62	0.005	18.41	0.006	18.33	0.007	SAO 1m
20230318	–	–	18.39	0.006	–	–	SAO 1m
20231012	–	–	18.43	0.011	–	–	SAO 1m
20231022	18.56	0.008	18.41	0.009	–	–	SAO BTA

Table A2. Summary of our B, V, R total magnitude estimates for DDO68 star-forming region Knot 2

Date	B	σ_B	V	σ_V	R	σ_R	Ref. Notes
19880214	19.74	0.018	–	–	19.38	0.022	CA3.5
19940502	–	–	–	–	19.36	0.021	INT 2.54m
19950207	19.75	0.029	19.63	0.027	–	–	NOT 2.56m
19971223	–	–	19.66	0.010	–	–	KeckII
19980217	19.76	0.028	19.62	0.039	–	–	KPNO 4m
20000503	19.77	0.024	19.65	0.028	19.41	0.036	VATT 1.8m
20040416	19.82	0.062	19.54	0.070	19.45	0.092	SDSS
20050112	–	–	19.67	0.014	19.43	0.013	SAO BTA
20070209	–	–	19.63	0.037	–	–	KP2.1 interp. from $V - g$
20090121	–	–	19.65	0.010	–	–	SAO BTA
20100502	–	–	19.56	0.077	–	–	HST
20110305	19.73	0.027	19.61	0.039	19.42	0.046	KPNO 0.9m
20130217	19.71	0.036	19.61	0.051	19.38	0.043	KPNO 0.9m
20150114	19.78	0.012	19.65	0.016	19.43	0.012	SAO BTA
20160307	–	–	19.60	0.014	–	–	SAO 1m
20160308	19.74	0.018	19.61	0.018	19.40	0.024	SAO 1m
20160407	–	–	19.58	0.015	–	–	SAO 1m
20160517	–	–	19.56	0.045	–	–	SAO 1m
20161022	–	–	19.60	0.032	–	–	SAO 1m
20161124	19.78	0.014	19.58	0.016	19.42	0.025	SAO 1m
20161224	–	–	19.56	0.018	–	–	SAO 1m
20161231	–	–	19.58	0.011	–	–	SAO 1m
20170418	–	–	19.57	0.009	–	–	CMO 2.5m
20170529	–	–	19.67	0.051	–	–	SAO 1m
20171116	19.74	0.011	19.66	0.014	19.42	0.011	SAO BTA
20180219	–	–	19.61	0.009	–	–	CMO 2.5m
20180405	19.73	0.018	19.58	0.037	19.38	0.022	SAO 1m
20180430	–	–	19.61	0.056	19.48	0.054	SAO 1m
20181011	–	–	19.63	0.068	–	–	SAO 1m
20190118	–	–	–	–	19.39	0.022	CMO 2.5m
20190203	–	–	19.58	0.018	–	–	SAO 1m
20191026	19.77	0.009	19.64	0.012	19.47	0.011	SAO BTA
20191125	–	–	19.58	0.021	–	–	SAO 1m
20200119	–	–	–	–	19.46	0.008	SAO BTA
20200120	19.75	0.008	19.67	0.009	–	–	SAO BTA
20200304	–	–	19.65	0.029	19.44	0.03	SAO 1m
20200426	–	–	–	–	19.46	0.012	SAO BTA
20201111	–	–	19.69	0.018	19.47	0.011	SAO BTA
20210514	–	–	19.60	0.017	–	–	SAO 1m
20210516	–	–	–	–	19.43	0.025	SAO 1m
20211202	–	–	19.67	0.013	19.45	0.014	SAO BTA
20220426	–	–	19.56	0.021	–	–	SAO 1m
20221025	–	–	19.57	0.019	19.45	0.027	SAO 1m
20221220	19.74	0.009	19.68	0.014	19.44	0.01	SAO BTA
20221225	19.77	0.016	19.67	0.013	19.43	0.015	SAO 1m
20230123	19.77	0.009	19.60	0.011	19.50	0.012	SAO 1m
20230318	–	–	19.57	0.013	–	–	SAO 1m
20231012	–	–	19.63	0.017	–	–	SAO 1m
20231022	19.75	0.012	19.61	0.020	–	–	SAO BTA

Table A3. Summary of our B, V, R total magnitude estimates for DDO68 SF region 3.

Date	B	σ_B	V	σ_V	R	σ_R	Ref. Notes
19880214	20.21	0.018	20.04	0.030	19.76	0.013	CA 3.5m phot
19940502	–	–	19.99	0.030	19.81	0.020	INT 2.54m phot
19950207	20.21	0.018	20.08	0.026	–	–	NOT 2.56m phot
19971223	–	–	20.09	0.010	–	–	KeckII
19980217	20.20	0.018	20.05	0.040	–	–	KPNO 4m
20000503	20.19	0.022	20.13	0.026	19.86	0.034	VATT 1.8m
20040416	20.22	0.050	20.01	0.057	19.90	0.072	SDSS phot
20041109	20.12	0.060	20.11	0.050	–	–	BTA cv (1)
20050112	20.30	0.030	20.19	0.013	19.89	0.013	BTA phot+cv (1)
20070209	–	–	19.89	0.040	–	–	KPNO 2.1m (1) interpol. from $V - g$
20080111	19.90	0.030	19.93	0.020	–	–	SAO BTA cv (1)
20080202	(19.47)	–	19.50	0.050	–	–	APO 3.5m cv (1)
20080204	19.51	0.070	(19.52)	0.050	–	–	SAO BTA cv (1)
20080328	(19.20)	0.100	19.30	0.100	–	–	MMT 6.5m cv (1)
20090121	–	–	19.55	0.008	–	–	SAO BTA phot+cv (1)
20100502	–	–	19.33	0.077	–	–	HST phot (1)
20110305	19.74	0.022	19.65	0.032	19.39	0.036	KPNO 0.9m
20130217	20.02	0.034	19.88	0.048	19.64	0.044	KPNO 0.9m
20150114	20.20	0.012	20.17	0.015	19.93	0.011	SAO BTA phot
20160307	–	–	19.96	0.013	–	–	SAO 1m phot
20160308	20.10	0.018	19.95	0.019	19.75	0.023	SAO 1m phot
20160407	–	–	19.95	0.015	–	–	SAO 1m phot
20160517	–	–	19.92	0.045	–	–	SAO 1m phot
20161022	–	–	19.99	0.024	–	–	SAO 1m phot
20161124	20.13	0.013	20.00	0.016	19.84	0.024	SAO 1m phot
20161224	–	–	19.89	0.019	–	–	SAO 1m phot
20161231	–	–	19.99	0.011	–	–	SAO 1m
20170418	–	–	19.96	0.008	–	–	CMO 2.5m phot
20170529	–	–	19.93	0.044	–	–	SAO 1m phot
20171116	20.20	0.011	20.13	0.013	19.93	0.011	SAO BTA phot
20180219	–	–	20.03	0.009	–	–	CMO 2.5m phot
20180405	20.18	0.017	19.98	0.035	19.84	0.022	SAO 1m phot
20180430	–	–	19.96	0.052	19.86	0.050	SAO 1m phot
20181011	–	–	20.05	0.066	–	–	SAO 1m phot
20190118	–	–	–	–	19.77	0.018	CMO 2.5m phot
20190203	–	–	20.00	0.018	–	–	SAO 1m phot
20191026	20.18	0.009	20.12	0.012	19.87	0.011	SAO BTA phot
20191125	–	–	19.99	0.021	–	–	SAO 1m phot
20200119	–	–	–	–	19.87	0.008	SAO BTA phot
20200120	20.19	0.008	20.16	0.009	–	–	SAO BTA phot
20200304	–	–	20.15	0.028	19.88	0.030	SAO 1m phot
20200426	–	–	–	–	19.89	0.011	SAO BTA phot
20201111	–	–	20.19	0.017	19.89	0.011	SAO BTA phot
20210514	–	–	20.03	0.018	–	–	SAO 1m phot
20210516	–	–	–	–	19.93	0.027	SAO 1m phot
20211202	–	–	20.18	0.013	19.91	0.013	SAO BTA phot
20220426	–	–	20.00	0.021	–	–	SAO 1m phot
20221025	–	–	19.95	0.020	19.85	0.026	SAO 1m phot
20221220	20.16	0.009	20.14	0.014	19.90	0.010	SAO BTA phot
221225	20.14	0.017	19.96	0.013	19.85	0.015	SAO 1m phot
230123	20.12	0.009	19.98	0.011	19.83	0.012	SAO 1m phot
230318	–	–	20.02	0.014	–	–	SAO 1m phot
231012	–	–	20.05	0.017	–	–	SAO 1m phot
231022	20.14	0.012	20.04	0.018	–	–	SAO BTA

(1) adopted from Pustilnik et al. (2017). 'cv' means the estimate from the spectrum convolution with the respective passband. See details in Pustilnik et al. (2017).

Table A4. Summary of our B, V, R total magnitude estimates for DDO68 star-forming region Knot 4

Date	B	σ_B	V	σ_V	R	σ_R	Ref. Notes
19880214	18.76	0.012	–	–	18.59	0.015	CA3.5
19940502	–	–	–	–	18.58	0.019	INT 2.54m
19950207	18.78	0.025	18.73	0.020	–	–	NOT 2.56m
19971223	–	–	18.70	0.008	–	–	KeckII
19980217	18.79	0.017	18.70	0.023	–	–	KPNO 4m
20000503	18.78	0.015	18.73	0.018	18.63	0.026	VATT 1.8m
20040416	18.83	0.033	18.71	0.060	18.63	0.065	SDSS
20050112	–	–	18.72	0.010	18.58	0.011	SAO BTA
20070209	–	–	18.73	0.032	–	–	KP2.1 interp. from $V - g$
20090121	–	–	18.73	0.008	–	–	SAO BTA
20100502	–	–	18.69	0.080	–	–	HST
20110305	18.79	0.019	18.74	0.027	18.60	0.032	KPNO 0.9m
20130207	18.80	0.023	18.75	0.031	18.63	0.030	KPNO 0.9m
20150114	18.81	0.010	18.73	0.010	18.64	0.009	SAO BTA
20160307	–	–	18.70	0.009	–	–	SAO 1m
20160308	18.78	0.014	18.68	0.013	18.58	0.019	SAO 1m
20160407	–	–	18.71	0.011	–	–	SAO 1m
20160517	–	–	18.69	0.03	–	–	SAO 1m
20161022	–	–	18.73	0.024	–	–	SAO 1m
20161124	18.81	0.010	18.73	0.012	18.63	0.018	SAO 1m
20161224	–	–	18.70	0.013	–	–	SAO 1m
20161231	–	–	18.69	0.008	–	–	SAO 1m
20170418	–	–	18.70	0.007	–	–	CMO 2.5m
20170529	–	–	18.75	0.032	–	–	SAO 1m
20171116	18.79	0.010	18.69	0.010	18.62	0.009	SAO BTA
20180219	–	–	18.75	0.007	–	–	CMO 2.5m
20180405	18.80	0.013	18.68	0.023	18.62	0.016	SAO 1m
20180430	–	–	18.74	0.037	18.61	0.035	SAO 1m
20181011	–	–	18.73	0.041	–	–	SAO 1m
20190118	–	–	–	–	18.61	0.017	CMO 2.5m
20190203	–	–	18.76	0.016	–	–	SAO 1m
20191026	18.80	0.008	18.68	0.010	18.61	0.010	SAO BTA
20191125	–	–	18.76	0.017	–	–	SAO 1m
20200119	–	–	–	–	18.58	0.007	SAO BTA
20200120	18.81	0.006	18.69	0.006	–	–	SAO BTA
20200304	–	–	18.75	0.020	18.63	0.023	SAO 1m
20200426	–	–	–	–	18.61	0.009	SAO BTA
20201111	–	–	18.68	0.009	18.60	0.008	SAO BTA
20210514	–	–	18.70	0.013	–	–	SAO 1m
20210516	–	–	–	–	18.61	0.017	SAO 1m
20211202	–	–	18.70	0.008	18.58	0.010	SAO BTA
20220426	–	–	18.72	0.016	–	–	SAO 1m
20221025	–	–	18.69	0.014	18.59	0.015	SAO 1m
20221220	18.80	0.006	18.68	0.009	18.57	0.007	SAO BTA
20221225	18.77	0.009	18.72	0.010	18.58	0.010	SAO 1m
20230123	18.81	0.006	18.78	0.007	18.61	0.010	SAO 1m
20230318	–	–	18.67	0.009	–	–	SAO 1m
20231012	–	–	18.75	0.013	–	–	SAO 1m
20231022	18.79	0.008	18.75	0.011	–	–	SAO BTA

Table A5. Summary of our B, V, R total magnitude estimates for DDO68 star-forming region Knot 5

Date	B	σ_B	V	σ_V	R	σ_R	Ref. Notes
19880214	19.23	0.010	–	–	18.99	0.011	CA3.5
19940502	–	–	–	–	19.01	0.019	INT 2.54m
19950207	19.19	0.024	19.08	0.018	–	–	NOT 2.56m
19971223	–	–	19.10	0.008	–	–	KeckII
19980217	19.18	0.014	19.16	0.017	–	–	KPNO 4m
20000503	19.21	0.013	19.15	0.012	19.00	0.016	VATT 1.8m
20040416	19.19	0.015	19.12	0.018	19.05	0.030	SDSS
20050112	–	–	19.09	0.009	18.99	0.011	SAO BTA
20070209	–	–	19.06	0.033	–	–	KP2.1 interp. from $V - g$
20090121	–	–	19.10	0.007	–	–	SAO BTA
20100502	–	–	19.13	0.080	–	–	HST
20110305	19.22	0.017	19.14	0.019	19.00	0.022	KPNO 0.9m
20130217	19.19	0.020	19.15	0.026	18.98	0.023	KPNO 0.9m
20150114	19.22	0.009	19.10	0.008	19.00	0.007	SAO BTA
20160307	–	–	19.09	0.007	–	–	SAO 1m
20160308	19.20	0.013	19.08	0.009	18.98	0.015	SAO 1m
20160407	–	–	19.09	0.008	–	–	SAO 1m
20160517	–	–	19.11	0.020	–	–	SAO 1m
20161022	–	–	19.10	0.017	–	–	SAO 1m
20161124	19.22	0.009	19.09	0.008	19.03	0.012	SAO 1m
20161224	–	–	19.12	0.011	–	–	SAO 1m
20161231	–	–	19.11	0.007	–	–	SAO 1m
20170418	–	–	19.12	0.006	–	–	CMO 2.5m
20170529	–	–	19.10	0.019	–	–	SAO 1m
20171116	19.22	0.010	19.12	0.009	19.04	0.009	SAO BTA
20180219	–	–	19.13	0.006	–	–	CMO 2.5m
20180405	19.20	0.010	19.09	0.016	19.01	0.010	SAO 1m
20180430	–	–	19.11	0.020	19.03	0.022	SAO 1m
20181011	–	–	19.11	0.026	–	–	SAO 1m
20190118	–	–	–	–	19.01	0.015	CMO 2.5m
20190203	–	–	19.09	0.014	–	–	SAO 1m
20191026	19.19	0.008	19.11	0.009	18.99	0.009	SAO BTA
20191125	–	–	19.08	0.016	–	–	SAO 1m
20200119	–	–	–	–	18.99	0.006	SAO BTA
20200120	19.20	0.006	19.08	0.004	–	–	SAO BTA
20200304	–	–	19.11	0.015	19.03	0.013	SAO 1m
20200426	–	–	–	–	19.00	0.009	SAO BTA
20201111	–	–	19.11	0.005	18.99	0.005	SAO BTA
20210514	–	–	19.10	0.011	–	–	SAO 1m
20210516	–	–	–	–	19.05	0.011	SAO 1m
20211202	–	–	19.09	0.005	19.00	0.009	SAO BTA
20220426	–	–	19.10	0.014	–	–	SAO 1m
20221025	–	–	19.11	0.011	19.05	0.010	SAO 1m
20221220	19.20	0.005	19.10	0.008	19.01	0.005	SAO BTA
20221225	19.20	0.008	19.11	0.008	19.04	0.008	SAO 1m
20230123	19.19	0.005	19.12	0.006	19.03	0.007	SAO 1m
20230318	–	–	19.10	0.007	–	–	SAO 1m
20231012	–	–	19.12	0.011	–	–	SAO 1m
20231022	19.20	0.008	19.11	0.008	–	–	SAO BTA

Table A6. Summary of our B, V, R total magnitude estimates for DDO68 star-forming region Knot 6

Date	B	σ_B	V	σ_V	R	σ_R	Ref. Notes
19880214	19.70	0.014	–	–	19.23	0.016	CA3.5
19940502	–	–	–	–	19.26	0.020	INT 2.54m
19950207	19.66	0.026	19.41	0.021	–	–	NOT 2.56m
19971223	–	–	19.36	0.008	–	–	KeckII
19980217	19.62	0.021	19.43	0.025	–	–	KPNO 4m
20000503	19.70	0.018	19.45	0.019	–	0.027	VATT 1.8m
20040416	19.67	0.042	19.44	0.064	19.33	0.072	SDSS
20050112	–	–	19.45	0.010	19.25	0.012	SAO BTA
20070209	–	–	19.40	0.041	–	–	KP2.1 interp. from $V - g$
20090121	–	–	19.50	0.008	–	–	SAO BTA
20100502	–	–	19.55	0.080	–	–	HST
20110305	19.63	0.021	19.43	0.028	19.25	0.032	KPNO 0.9m
20130207	19.60	0.026	19.36	0.032	19.19	0.030	KPNO 0.9m
20150114	19.68	0.010	19.39	0.010	19.21	0.008	SAO BTA
20160307	–	–	19.41	0.010	–	–	SAO 1m
20160308	19.63	0.015	19.41	0.014	19.19	0.019	SAO 1m
20160407	–	–	19.42	0.012	–	–	SAO 1m
20160517	–	–	19.36	0.031	–	–	SAO 1m
20161022	–	–	19.46	0.024	–	–	SAO 1m
20161124	19.63	0.012	19.39	0.013	19.25	0.018	SAO 1m
20161224	–	–	19.43	0.015	–	–	SAO 1m
20161231	–	–	19.44	0.010	–	–	SAO 1m
20170418	–	–	19.40	0.007	–	–	CMO 2.5m
20170529	–	–	19.47	0.032	–	–	SAO 1m
20171116	19.67	0.010	19.42	0.010	19.33	0.009	SAO BTA
20180219	–	–	19.40	0.008	–	–	CMO 2.5m
20180405	19.69	0.015	19.42	0.026	19.28	0.016	SAO 1m
20180430	–	–	19.47	0.043	19.29	0.038	SAO 1m
20181011	–	–	19.47	0.048	–	–	SAO 1m
20190118	–	–	–	–	19.25	0.023	CMO 2.5m
20190203	–	–	19.50	0.016	–	–	SAO 1m
20191026	19.64	0.008	19.42	0.010	19.24	0.010	SAO BTA
20191125	–	–	19.49	0.018	–	–	SAO 1m
20200119	–	–	–	–	19.28	0.007	SAO BTA
20200120	19.65	0.007	19.52	0.006	–	–	SAO BTA
20200304	–	–	19.51	0.021	19.33	0.022	SAO 1m
20200426	–	–	–	–	19.26	0.010	SAO BTA
20201111	–	–	19.46	0.010	19.25	0.008	SAO BTA
20210514	–	–	19.49	0.014	–	–	SAO 1m
20210516	–	–	–	–	19.27	0.018	SAO 1m
20211202	–	–	19.41	0.008	19.25	0.010	SAO BTA
20220426	–	–	19.49	0.017	–	–	SAO 1m
20221025	–	–	19.42	0.015	19.30	0.018	SAO 1m
20221220	19.62	0.007	19.46	0.010	19.30	0.008	SAO BTA
20221225	19.61	0.012	19.39	0.011	19.25	0.011	SAO 1m
20230123	19.66	0.007	19.49	0.008	19.27	0.010	SAO 1m
20230318	–	–	19.49	0.011	–	–	SAO 1m
20231012	–	–	19.47	0.014	–	–	SAO 1m
20231022	19.63	0.010	19.44	0.011	–	–	SAO BTA